Salinity and Stratification at the Sea Ice Edge (SASSIE): An oceanographic field campaign in the Beaufort Sea

Kyla Drushka[1], Elizabeth Westbrook[2], Frederick M. Bingham[2], Peter Gaube[1], Suzanne Dickinson[1*], Severine Fournier[3*], Viviane Menezes[4*], Sidharth Misra[3*], Jaynise Perez[1*], Edwin J. Rainville[1*], Julian J. Schanze[5*], Carlyn Schmidgall[1,6*], Andrey Shcherbina[1*], Michael Steele[1*], Jim Thomson[1*], Seth Zippel[7*]

[1] Applied Physics Laboratory, University of Washington, Seattle WA, 98105, United States

[2] Department of Physics & Physical Oceanography, University of North Carolina Wilmington, Wilmington NC, 28412, United States

[3] Jet Propulsion Laboratory, California Institute of Technology, Pasadena, CA 91109, USA

[4] Woods Hole Oceanographic Institution, Falmouth, MA 02543, United States

[5] Earth and Space Research, Seattle, WA, 98105, United States

[6] School of Oceanography, University of Washington, Seattle WA, 98105, United States

[7] Oregon State University College of Earth Ocean and Atmospheric Sciences, Corvallis, OR, 97331, United States

[*] These authors listed in alphabetical order

Correspondence to: Peter Gaube (pgaube@uw.edu)

Abstract. As our planet warms, Arctic Sea ice coverage continues to decline resulting in complex feedbacks with the climate system. The core objective of NASA's Salinity and Stratification at the Sea Ice Edge (SASSIE) mission is to understand how ocean salinity and near-surface stratification affect upper ocean heat content, and thus sea ice freeze and melt. SASSIE specifically focuses on the formation of Arctic Sea ice in autumn. The SASSIE field campaign in 2022 collected detailed observations of upper ocean properties and meteorology near the sea ice edge in the Beaufort Sea using ship-based and piloted and drifting assets. The observations collected during SASSIE include vertical profiles of stratification up to the sea surface, air-sea fluxes, and ancillary measurements that are being used to better understand the role of salinity in coupled Arctic air-sea-ice processes. This publication provides a detailed overview of the activities during the 2022 SASSIE campaign and presents the publicly available datasets generated by this mission, introducing an accompanying repository that highlights the numerical routines used to generate the figures shown in this manuscript.

1 Introduction

1.1 Background

Sea ice extent in the Arctic Ocean has declined dramatically over the past decades. As a result of climate change, autumn ice advance is slower and occurs later, while summer ice retreat is faster and occurs earlier (Stroeve et al., 2014; Stroeve and Notz, 2018). The result is a lengthening open-water period each year, leading to changes in air-sea heat and momentum fluxes, the freshwater cycle, surface albedo feedback, primary production, and regional and global climate as well as human and ecological health (Lannuzel et al., 2020). Understanding the dynamics that govern the spatial and temporal patterns of sea ice formation is critical to understanding and predicting the impacts of the changing Aarctic cryosphere.

Salinity controls stratification in the cold Arctic Seas, enabling the uniquely polar phenomenon of colder, less-dense fresher waters situated above warmer, denser saltier waters. Variations in upper ocean salinity and the resulting stratification modulate the surface ventilation of stored subsurface heat, which can affect upper ocean temperature and thus sea ice formation and melt (e.g., Smith et al., 2018). During summer, melting sea ice leaves a layer of fresh, cold water at the ocean surface (Dewey et al, 2017). By mid-September, sea ice extent reaches a minimum: melting stops, and the ice edge begins to advance. The freshwater deposited by melting sea ice during its seasonal retreat may increase near-surface stratification, suppressing upward mixing of heat from the warmer subsurface waters and thereby enhancing surface cooling, as shown by Crews et al. (2022). Increased stratification from melted sea ice may precondition the ocean for autumn sea ice formation, but there are very few in situ ocean and sea ice observations of this connection.

Salinity and Stratification at the Sea Ice Edge (SASSIE) is a NASA physical oceanography mission that aims to clarify the role of salinity and upper ocean stratification in the Arctic Ocean. The primary goal of SASSIE is to better understand how the salinity anomalies generated by summer ice melt in the Western Arctic evolve in space and time and ultimately how they affect the upper ocean structure and the formation of sea ice in the early fall. This paper describes data collected during the SASSIE field campaign that took place in August-October 2022 in the Beaufort Sea, including in situ measurements collected from a ship and a suite of uncrewed and drifting platforms as well as remote sensing measurements collected from an aircraft. Satellite measurements (for instance, sea surface salinity, temperature, and height; surface winds; sea ice concentration) and model simulations are also a crucial part of the SASSIE mission data but are not addressed here.

1.2 Campaign overview

The SASSIE campaign focused on capturing three regimes in the Beaufort Sea, a region characterized by strong near-surface salinity stratification. Late summer sea ice melt was sampled with a fleet of four Wave Gliders that traveled progressively northward from mid-August to early September as the sea ice retreated (Figure 1a, b, and Table 1).

SASSIE's intensive observing period, from early September to early October, centered around the ship- and aircraft-based campaign during the transition between the summer melt season and fall freeze-up (Figure 1c, d). This main phase of the campaign focused on the region of the Beaufort Sea bounded by the shelf-break to the south and the sea ice edge to the north, between 154°W and 145°W (Figure 2). Following the intensive ship and airborne campaigns, the early part of the freeze-up was sampled with several floats and drifters that remained in the water after the ship departed.
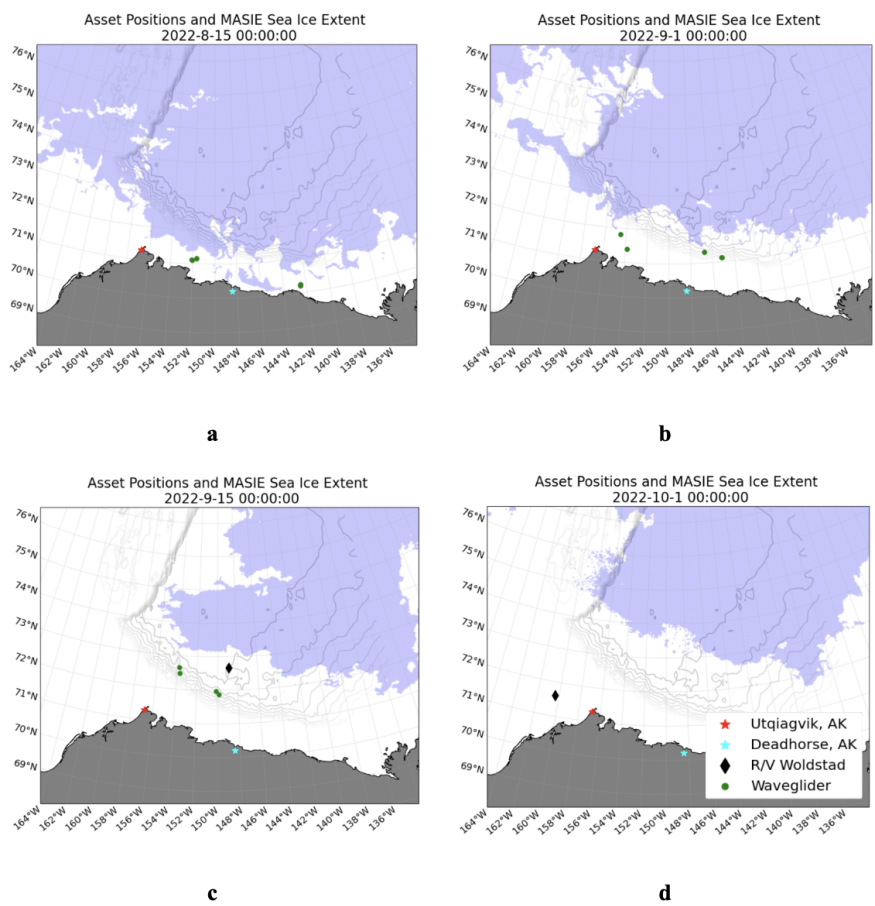
Figure 1: Sea ice coverage, indicated by blue coloring.extent from the MASIE-NH product (US National Ice Center, 2010) for (a) 15 August, (b) 1 September, (c) 15 September, and (d) 1 October 2022. "Sea ice extent" refers to the area where the

80 MASIE-NH product indicates greater than 0 percent ice concentration. **The positions of the RV *Woldstad* (black diamond) and the Wave Gliders (green circle) on each date are shown. Bathymetry contours from 1000 to 6000 m (gray lines) from the ETOPO2 product (Smith & Sandwell v. 8.2: 1/30-degree topography and bathymetry) are shown for reference.**
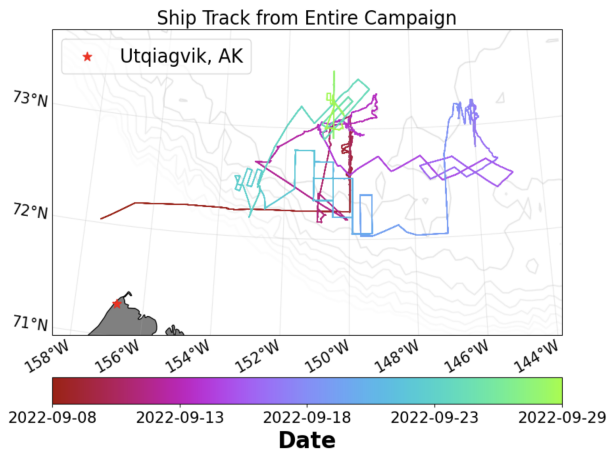
Figure 2 The track of the RV *Woldstad* throughout the SASSIE campaign, colored by date. Bathymetry data (grey lines)
85 **from 1000 to 6000 m at an interval of 300 m added for reference.**

The major daily activities of the SASSIE campaign are summarized in Table 1. An animated depiction of the platforms is included in the supplemental materials.

Date (2022)	Event
August	
12-14	Wave Glider deployments from RV *Ukpik*.
28-29	RV *Woldstad* mobilization in Homer, AK.
30 - Sept 5	RV *Woldstad* transit from Homer, AK to Nome, AK with only crew aboard.
September	
5	RV *Woldstad* departs Nome with 12 scientists and 6 crew. Shipboard sensors begin collecting data.
7	RV *Woldstad* rounds Point Barrow.
8	RV *Woldstad* enters the study area and begins play #1: ice and open water survey. Four ALTO floats and 1 HydroBuoy deployed.
9	Five SWIFTs, 2 HydroBuoys deployed.

10	Under Ice Float deployed. JetSSP deployment #1.
11	Four Wave Gliders recovered. One ALAMO float and 1 HydroBuoy deployed. JetSSP deployment #2. Aircraft flight #1.
12	Four Wave Gliders redeployed and 5 SWIFTs recovered.
13	Two ice stations. One HydroBuoy deployed. Play #1 ends as the ship exits heavy ice cover.
14	Play #2 (zig-zag open water survey) begins. Aircraft flight #2.
15	One ALAMO float and 2 HydroBuoys deployed.
16	Play #2 ends. Play #3 (ice survey) begins. Aircraft flight #3.
17	1 HydroBuoy deployed. Two SWIFTs deployed and recovered. JetSSP deployment #3. Aircraft flight #4
18	Two SWIFTs deployed and recovered. Aircraft flight #5. Play #3 ends.
19	Wave Glider 245 recovered. Play #4 (drifter-following survey boxes) begins. One ALAMO, 2 HydroBuoys, and 2 SWIFTs deployed.
20	JetSSP deployment #4.
21	Wave Glider 245 redeployed. JetSSP deployment #5. One SWIFT deployed.
22	Wave Gliders 153 and 130 recovered. One SWIFT deployed.
23	Play #4 ends. Four SWIFTs recovered.
24	Wave Gliders 153 and 130 redeployed.
25	Wave Glider 247 recovered and redeployed. Play #5 (Repeated ice-open water transect) begins. Two HydroBuoys, 2 SWIFTs, and 1 ALAMO float deployed. JetSSP deployment #6.
26	JetSSP survey #7. One SWIFT deployed.
27	One SWIFT deployed and recovered.
28	Four Wave Gliders and 3 SWIFTs recovered.
29	Play #5 ends. Transit to Nome, AK begins.
October	
1	Air-sea flux sensors turned off.
2	Salinity snake recovered.

3	RV *Woldstad* arrives in Nome, AK. Science party disembarks. Ship transits to Homer with only crew aboard.
10	RV *Woldstad* demobilization in Homer, AK.

Table 1. A timeline of SASSIE events. Dates are local time. All other dates and times in this paper are in UTC. The plays referred to in the table are described in Sect. 3.

90   A major objective of the SASSIE mission is to deliver quality-controlled data products to NASA's Physical Oceanography Distributed Active Archive Center (PO.DAAC) to foster broad utilization of the data within the broader scientific community. This paper outlines the campaign and describes the 15 SASSIE datasets archived at the PO. DAAC and available at https://podaac.jpl.nasa.gov/SASSIE. Python notebooks to download, read and visualize the data are available at the SASSIE's Data Visualization GitHub page: https://doi.org/10.5281/zenodo.8308513. Sect. 2

95   describes the data and processing for each of the platforms deployed during SASSIE; Sect. 3 details the five "plays" that distinguish different periods of the research cruise; Sect. 4 gives information about how SASSIE data can be accessed; and Sect. 5 gives definitions of the abbreviations used in this paper.

2 Data

2.1 Research vessel and ship-deployed instruments

100   The ship-based sampling of the SASSIE program was carried out on the RV *Woldstad* (Figure 3), a 121' deep-draft steel vessel operated by Support Vessels of Alaska. This section describes all measurements collected from the RV *Woldstad.* A thermosalinograph (TSG) and S-band navigation radar are permanently installed on the vessel, while the SASSIE team supplied all other shipboard instruments.
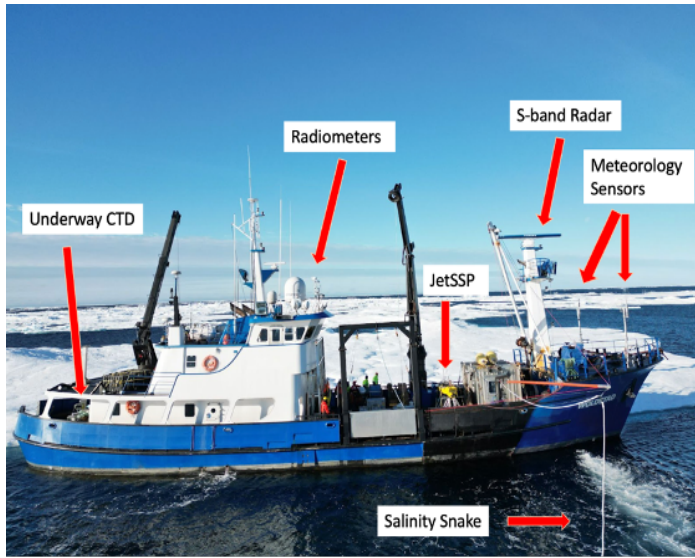
Figure 3. The RV *Woldstad*. The photo was taken during the ice station on 13 September 2022. Note: 1) the boom for the salinity snake protruding from the starboard side of the ship in the foreground; 2) two air-sea flux masts on the bow; 3) the radiometers above the bridge; 4) the JetSSP ready for deployment on the foredeck; 5) uCTD winch on the stern. 7) S-band radar antenna on the mast.

2.1.1 Thermosalinograph (Drushka, 2023a)

The shipboard TSG system pumped water from an intake on the ship's hull at around 4 m depth through a SBE38 temperature sensor, a vortex debubbler, and finally a SBE21 SeaCAT TSG. Temperature and conductivity data were logged every 10 seconds~~minute~~ using SeaSave software. Temperature measurements were made from both the SBE21 and SBE38 instruments: the SBE21 temperature measurement is only used for the salinity computation; the SBE38 temperature more accurately reflects the ocean temperature because the sensor measures seawater prior to it going through the TSG.

Temperature data were quality controlled by removing values greater than 15°C (<0.001% of data) and spikes, defined as anomalies larger than 0.3°C over 1 minute (<0.005% of data). Salinity data were quality controlled by removing values smaller than 22 (<0.03% of data) and negative spikes, defined as anomalies larger than –0.08 over 1 minute (<0.5% of data). Comparisons of salinity measurements from the TSG and from the three CTD sensors on the JetSSP (see section 2.2.2), during periods while the upper ocean was well-mixed and all JetSSP sensors agreed, indicate that the ship's TSG had a –0.05 (fresh) bias. This bias was corrected in the final data product.

The large fluctuations observed in the temperature and salinity time series (Figure 4) primarily reflect spatial variability captured as the ship moved between open regions south of the ice edge and areas with low to moderate ice

cover. Surface waters in the SASSIE domain were typically warmer and saltier in open water (1 to 2.5°C, 26 to 28) and cooler and fresher within the ice (-1 to 0°C, <26) ~~within the ice~~ (Figure 5). An exception is the strong variability seen from 19-23 September, when the ship was in open water and sampled a region with strong fronts (Figure 4).
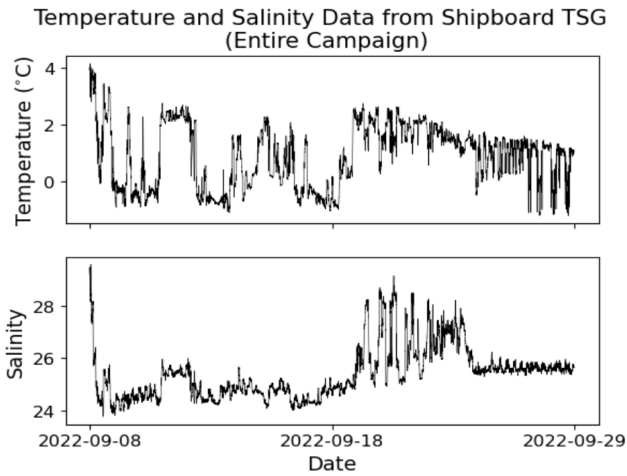
Figure 4. Temperature (top) and salinity (bottom) records from the ship's thermosalinograph (TSG) during the SASSIE campaign.
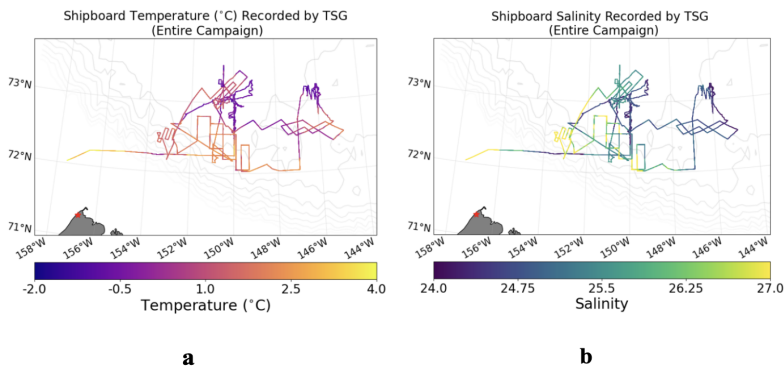
Figure 5. (a) Temperature and (b) salinity from the shipboard TSG along the ship track from the entire SASSIE campaign.

 2.1.2 Meteorology and Air-Sea Fluxes (~~Menezes and~~ Zippel _and Menezes_, 2023)

Shipboard atmospheric measurements (wind speed and direction, shortwave and longwave radiation, barometric pressure, air humidity, and air temperature) were made almost continuously throughout the SASSIE cruise from two

masts (on the port and starboard side of the bow, which were instrumented with the WHOI DCFS (Direct Covariance Flux System) system, Metek uSonic-3, and Licor 7500; Figure 6) and from a barometer and radiometers mounted

140 above the ship's wheelhouse (Table 2). These measurements are used to calculate air-sea heat and momentum fluxes using both the direct covariance method (Edson et al., 1998) and the traditional bulk flux algorithm from state variables. This dual strategy was chosen because the presence of sea ice modifies the surface roughness and surface temperature, making the efficacy of traditional bulk flux algorithms within 5 km of ice cover uncertain (Fairall and Markson, 1987).

145

Sensor	Variables measured	Sensor location and height above water level	Notes
DCFS system: Gill R3 + Systron and Donner IMU	Wind speed, wind direction, sonic temperature, wind stress, sonic temperature flux, xyz acceleration, xyz gyro rates,	Port bow; 7.9 m	Sporadic freezing of sensor head
Metek uSonic-3 omni	Wind speed, wind direction, sonic temperature, wind stress, sonic temperature flux	Starboard bow; 7.9 m	
Licor 7500	Moisture, air temperature, air pressure	Port bow; 7.0m (sensor head)	Sporadic freezing of sensor head
Vaisala HMP60	Relative humidity (RH), air temperature	Wheelhouse 10 m	Both port and starboard RH sensors failed.
Setra 278 Barometer	Atmospheric pressure	Wheelhouse; 10 m	
Kipp and Zonen CMP21 pyronometer	Downwelling shortwave radiation	Wheelhouse; 10 m	
Kipp and Zonen CGR4 pyrgeometer	Downwelling longwave radiation	Wheelhouse; 10 m	

Table 2. Shipboard mMeteorological sensors deployed during SASSIE. Ship position and navigation data and sea surface temperature from the Salinity Snake were also used to compute bulk flux estimates.
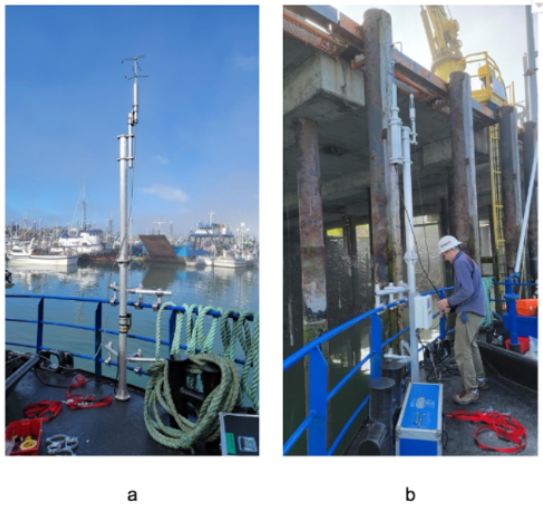
Figure 6. (a) Starboard bow air-sea flux mast instrumented with Metek (a); **(b)** port bow mast instrumented with DCFS system and Licor (b).

Detailed quality control processes for the meteorological measurements are as follows:

Wind speeds: Mean wind speeds between the two anemometers differed by as much as 10% due to flow distortion around the ship's superstructure. The ship's flow distortion was found to be a strong function of apparent wind angle, with a large blockage caused from the forward radar mast (roughly +150 degrees from bow for the port-side sensor, -150 degrees from bow for the starboard-side sensor). A linear average of the two wind speeds would effectively distribute the bias evenly between the two sensors. A study using multiple wind sensors on a buoy showed a similar bias pattern with apparent wind angle (Schlundt et al., 2020) and highlighted that the difference between the two sensors' wind speeds was distributed such that the upwind sensor accounted for roughly 75% of the difference, and the downwind sensor accounted for roughly 25% of the wind speed difference. We followed these percentages of (Schlundt et al., 2020), reducing the upstream sensor by 75% of the wind speed difference, and increasing the downwind sensor by 25% of the wind speed difference, with the error determined from the average percentage difference between the two wind sensors at relative direction from +100 to -100 degrees. For directions where one sensor was obstructed by the radar mast (near +/-150 degrees), this correction was not considered (since the nature of the flow distortion was different), and the unobstructed sensor data was used uncorrected. An ad-hoc correction was applied to each mean wind estimate informed by previous ship and buoy computational fluid dynamics studies to reconcile the 10% mean wind speed errors as a function of ship-relative direction. True wind speeds and directions

are then estimated by subtracting the ship's velocity vector (estimated from the navigation data). The two sonic anemometer time series are de-spiked, and averaged to form a blended wind speed product.

Air temperature: The Vaisala data reported intermittently and had numerous spikes. The Licor temperature was recorded from a sensor in the instrument's electronics box, which was not radiation shielded and so exhibited high bias under strong shortwave radiative forcing. Sonic temperature measured from anemometers is known to differ from the true temperature due to the sensitivity of the speed of sound in air to water vapor. In most cases, sonic temperature is subject to sensor drift to a variety of factors, including the temperature of the sensor itself. For this deployment, the Metek sonic temperature was relatively stable due to the generally low absolute humidity in cold temperatures, and because the sensor head was temperature controlled through a heating element. This lack of temperature drift was apparent through a high correlation between the night-time Licor air temperature (when the Licor sensor was not subject to radiative heating) and the Metek sonic temperature. Day-time air temperature values between the Licor and Metek were still correlated, however showed a bias with the Licor temperatures larger than the Metek temperatures consistent with radiative heating of the Licor sensor. ~~The Metek sonic temperature was stable due to the heating of the sensor, but exhibited a general bias and responded to changes in the speed of sound due to moisture~~. A corrected temperature product was created by finding the constant offset between the Metek Sonic temperature and the night-time Licor air-temperatures values to replace the biased day-time Licor air-temperature values. ~~–~~This~~e~~ corrected temperature product resulted in much better agreement between bulk and direct buoyancy fluxes than if any~~either~~ of the three raw air temperatures were used uncorrected. ~~The blended temperature product combines data from these three sensors.~~ Figure 7 shows wind speed and direction measurements, colored by air temperature.
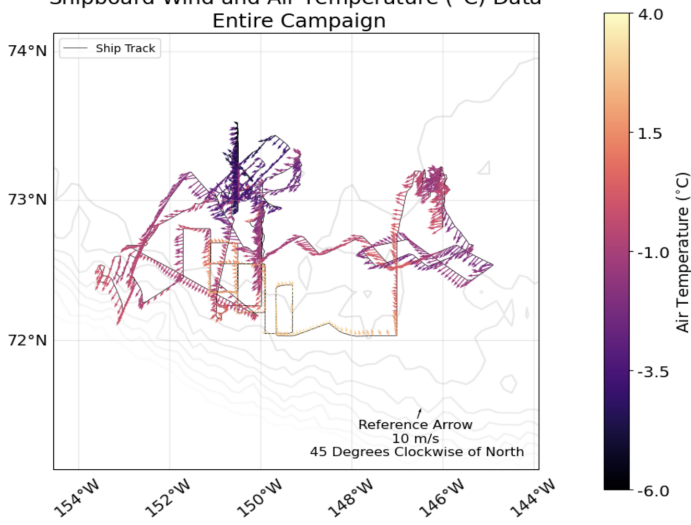
Figure 7. Wind speed and direction measured from the RV *Woldstad* throughout the SASSIE campaign. The arrows are colored by air temperature. Bathymetry contours are shown for reference.

Direct momentum fluxes: Direct covariance estimates of the wind stress are made following the Edson et al. (1998) method. Raw wind speed data are corrected using the acceleration/gyro system to remove the contamination from ship pitch, heave, and tilt motions.

Inertial dissipation fluxes: Estimates of total kinetic energy (TKE) dissipation rate are made by fitting a theoretical model to the measured power spectra of vertical velocity from the sonic anemometers. A TKE balance is assumed , and inverted for wind stress as described in Fairall et al. (1990) and Edson et al. (1991).

Bulk fluxes: Bulk fluxes are estimated from the COARE 3.5 algorithm (Edson et al., 2013) using blended wind speed, air temperature products, radiometer measurements, and SST (see Section 2.1.1). Due to the failure of the Vaisala RH sensors and the noise of the Licor 7500, bulk fluxes are run with a constant RH (RH = 89) informed by previous cruises (Persson et al. 2018). Errors in the latent heat flux are reported as the range of fluxes estimated from the range of RH values reported in Persson et al. (2018) (RH= 70 to RH=100). Figure 8 provides a summary of surface flux measurements throughout the campaign.
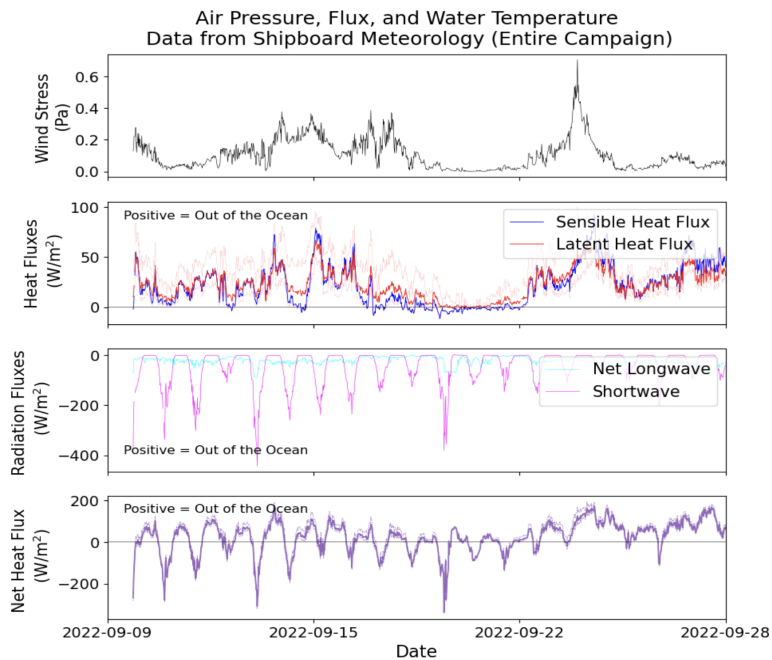
Figure 8. Surface flux measurements measured from RV *Woldstad*. (a) Wind stress (Pa). (b) Latent (red) and sensible (blue) heat flux (W/m²), with faintly colored~~dashed~~ lines showing uncertainty of latent heat from RH values. (c) Net longwave (blue) and shortwave (pink) radiation (W/m²). (d) Net heat flux (solid line) and its uncertainty (faint~~dashed~~ lines).

Winds in the SASSIE domain were predominantly easterly (Figure 7). SASSIE captured three periods of relatively strong winds (~14-15 September, 17-18 September, 24 September) that drove turbulent cooling, and a period of very weak winds (19-20 September) during which sensible and latent fluxes were near zero. Throughout the campaign, downwelling radiation remained fairly consistent. As the daily peak in solar radiation decreased during the transition to autumn, net heat flux transitioned from predominantly warming the ocean in early September to cooling the ocean starting around 22 September (Figure 8).

2.1.3 Salinity snake and FDOM/CDOM (Schanze, 2023)

To measure the very near surface salinity without contamination from the ship's wake, a salinity snake (Ho and Schanze, 2020) was deployed on the RV *Woldstad* during SASSIE The salinity snake instrument consists of four main components: a boom, an intake hose, a pump, and a shipboard apparatus. A boom with a halyard is deployed to the starboard side of the vessel, which is used to position a flexible steel-reinforced rubber hose outside the wake of the ship. Water is pumped from the surface of the ocean at approximately 0.05 m depth, passes through a de-bubbler system and enters a Seabird SBE-45 TSG (note that this is completely independent from the TSG that is permanently installed on the RV *Woldstad*). Water then passes through a Turner Designs C-FLUOR fluorometer with RS232 output. The fluorometer yields measurements of fluorescent dissolved organic matter (FDOM), which is a proxy measurement of colored dissolved organic matter (CDOM). The FDOM probe is factory calibrated and needs no further calibration. A SBE56 temperature logger inside the seawater end of the intake hose makes a continuous measurement of water temperature at ~0.05 m depth.

Ancillary data generated by the salinity snake system include the flow rate, pump suction, and instrument pressure. These values are used in the quality control of the salinity data to ensure a flow rate between 0.5 - 3 l min^{-1} was present at the instrument.

The salinity snake collected data throughout the SASSIE cruise (Figure 9) and captured the same general temperature and salinity patterns as the shipboard TSG (Figure 4b). FDOM patterns (Figure 10) are distinct from those of temperature or salinity.
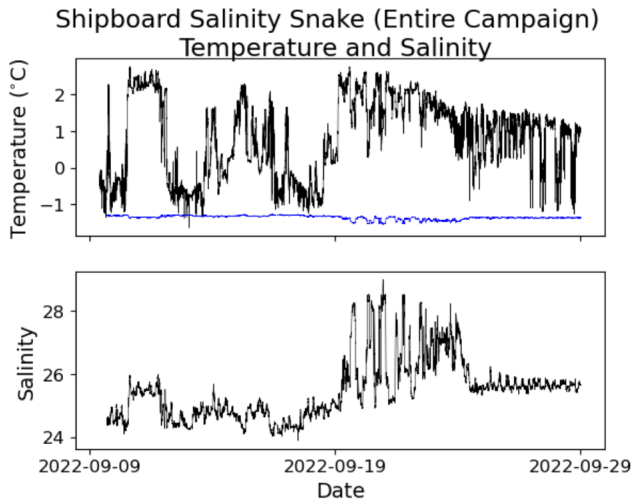
Figure 9. Shipboard salinity snake temperature and salinity measurements throughout the entire SASSIE campaign. The blue line indicates the freezing temperature of the water.
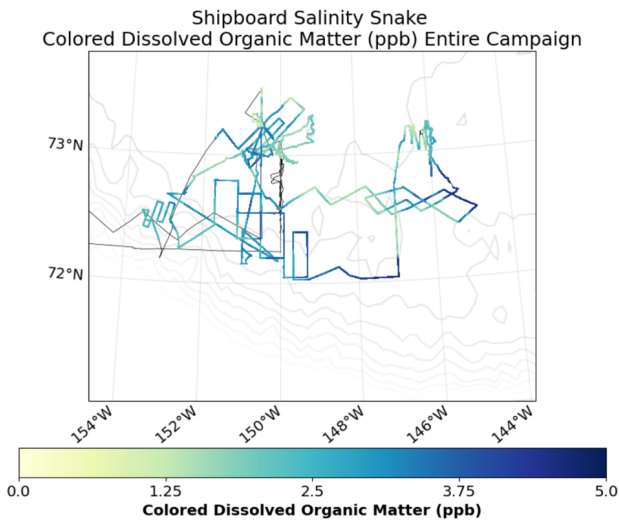
Figure 10. Colored dissolved organic matter measurements from the shipboard salinity snake throughout the SASSIE campaign. Ship track (black line) and bathymetry contours from 1000m to 6000m shown for reference.

2.1.4 ADCP (Gaube, 2023)

A hull-mounted 300 kHz Teledyne Workhorse Mariner ADCP was used to estimate vector current profiles from ~ 5 m to ~70 - 120 m depth depending on the concentration of scattering material in the water. The ADCP was operated in narrowband mode and ADCP measurements were logged using VMDAS software every 1 minute. Unfortunately, theis ship's heading sensor was not functioning correctly and so the heading could not be correctly removed from the current vectors, thus vector ocean velocity estimates could not be made. Vertical current shear magnitude was estimated as the vertical derivative of current speed without any heading corrections and is archived in the data collection. The vertical gradient was computed on a vertical grid located at the midpoints of ADCP bins; currents larger than 2 m/s were flagged as errors and removed from the data prior to computing the vertical gradient. Estimates of the vertical ocean current shear were produced and are archived in the data collection, but are not displayed here. Figure 11 illustrates the patterns of vertical shear in the upper ocean. The largest values generally correspond to periods with stronger winds (e.g., Figure 7). Areas of alternating positive and negative shear were also observed, for instance south of 73°N from 152°W to 149°W, consistent with the strong sub-mesoscale fronts observed in the upper ocean temperature and salinity data (play #4; see section 3.4).
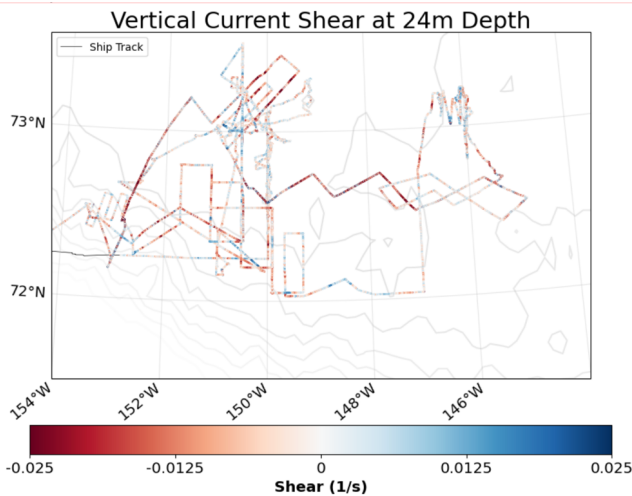
Figure 11. A map of vertical current shear at 24m depth collected by the ADCP on the R/V *Woldstad* throughout the SASSIE campaign.

2.1.5 uCTD and cCTD Measurements (Schmidgall, 2023; Pérez 2023)

The underway CTD (uCTD; Figure 121a) system was used to measure vertical profiles of temperature and conductivity (and thus salinity and density) at survey speed throughout the SASSIE experiment. The uCTD, a platform that was developed and built at APL-UW, was primarily deployed in open water, whereas in areas with sea ice a SonTek Castaway CTD (cCTD; Figure 121b) was more typically used. A total of 2,518 CTD casts were collected in the Beaufort Sea (Figure 121), 2,246 of which were made with the APL uCTD.

a        b

Figure 12~~12~~. (a) uCTD and (b) cCTD instruments. The uCTD has a total length of 1.08 m and the cCTD a total length of 0.20 m.

a        b
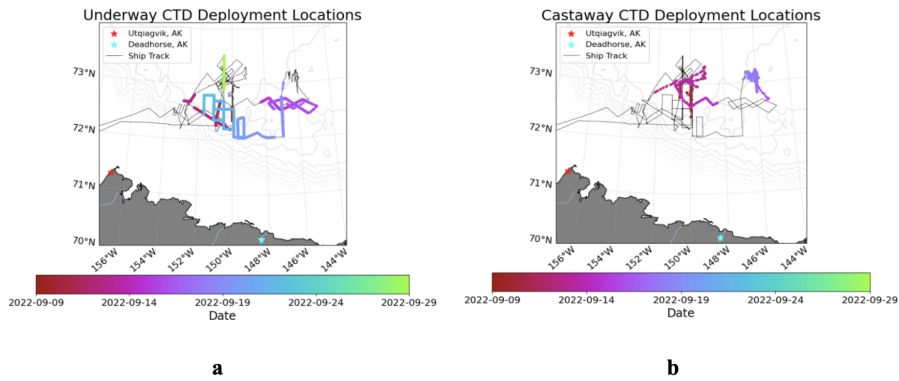
Figure 13~~21~~. Locations of (a) uCTD ~~(a)~~ and (b) cCTD ~~(b)~~ profiles colored by date, along with the ship track (black line).

Individual casts are hard to distinguish as they are close together. Bathymetry data (gray lines) added for reference.

The uCTD consists of an armored and faired RBR –concerto CTD sensor (RBR, Ottawa, Canada) that was lowered and raised using an electric fishing reel, which was mounted to a stand at the aft starboard side of the RV *Woldstad* (~~Figure 11~~2a). The line was extended several meters to the aft starboard side with a boom to sample away from the ship's prop wash. Nonetheless, it must be assumed that the upper ~4 m of the ocean behind the ship were well mixed;

280 those data must be used with caution. The RBR concerto recorded measurements of conductivity, temperature, and pressure at 32 Hz. The average fall rate of the sensor was 2.1 m s⁻¹, giving a vertical sampling interval of ~6.5 cm. The horizontal spacing between continuous casts averaged ~0.8 km and the average depth of the casts was 100 m, with some casts reaching 200 m.

285 The uCTD data were offloaded via the RBR Ruskin software, quality controlled, and gridded onto a uniform vertical grid with spacing of 0.1 m. Only the data from the down casts are retained for analysis. The uCTD data were collocated with data from the shipboard navigation system to provide position information for each cast. The uCTD was deployed continuously (in "tow-yo" mode) as the ship steamed at 1-4 m s⁻¹ whenever conditions permitted: typically, in areas with sufficiently low ice cover that the ship could maneuver between floes. In slightly heavier ice cover (10-30% sea

290 ice concentration), when continuous profiling was not safe, the ship typically stopped every 30 minutes and a single uCTD cast was collected. During rough seas (wind speeds greater than around 10 m s⁻¹), the uCTD could not be deployed.

295 In cases where the uCTD could not be used, profiles were instead collected with thea cCTD – typically every 30 minutes as the ship was underway. A total of 272 total cCTD casts were collected (Figure 132b). The cCTD is a small, rugged, and technically advanced CTD designed for profiling to depths of up to 100 m (Figure 1212b). It records temperature, conductivity, and pressure at 5 Hz (resulting in ~0.3 m vertical resolution), as well as GPS position information for each cast. Casts reached an average depth of 45 m, with considerable variance depending on the ship's speed and amount of line used (Figure 143, 154). The accuracy of the cCTD salinity measurements is roughly 0.1.

300 Surface data from the cCTD were compared to TSG measurements to assess the accuracy of the cCTD measurements at the surface; profiles for which the cCTD temperatures were more than ± 2°C or the cCTD salinities were more than ±1.5 different from the nearest TSG measurements were discarded.Surface data were validated against TSG measurements for quality control assessment.

305 The uCTD and cCTD measurements collected during SASSIE reveal a wealth of horizontal and vertical upper ocean structure (Figures 143,154,165), including signatures of Pacific summer water (temperature maxima around 50 m depth), near-surface temperature maxima typical of the region (Jackson et al., 2010), and strong lateral salinity gradients in the upper 20 m.

a

b

310
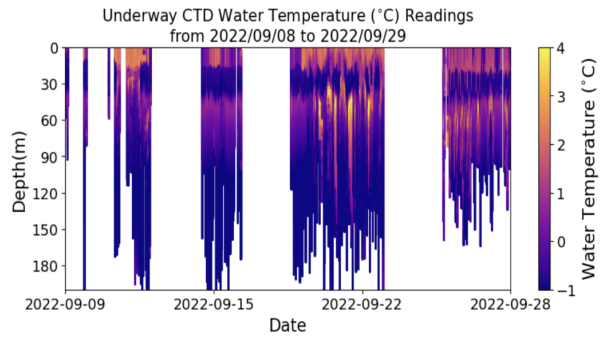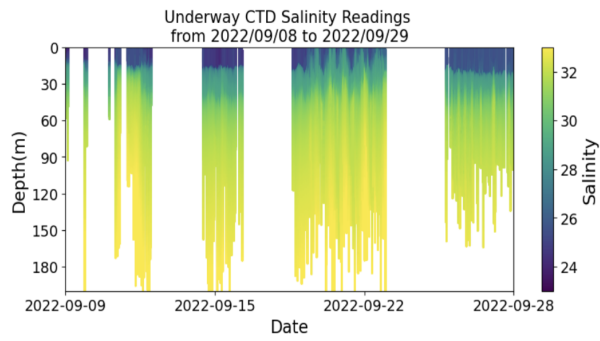
Figure 1~~4~~3. (a) temperature and (b) salinity profiles measured by the uCTD.
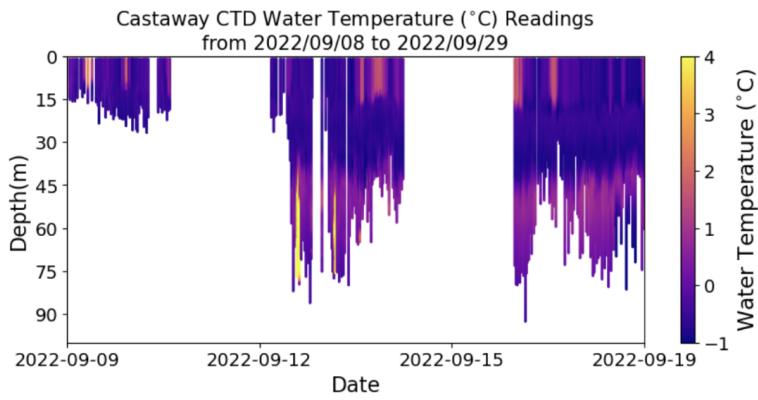
a
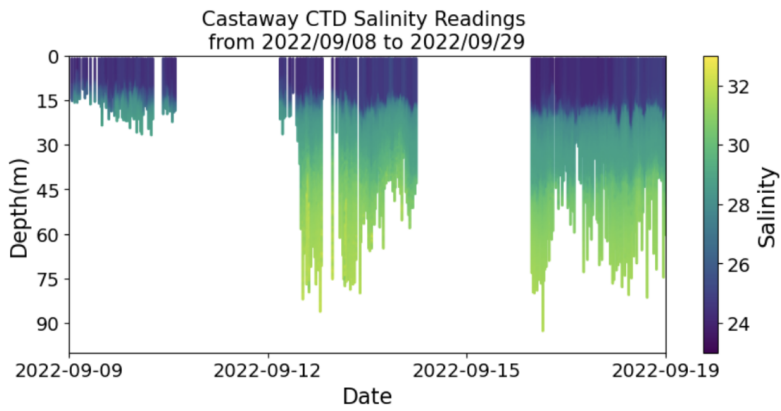
b

Figure 1~~5~~4. (a) temperature and (b) salinity profiles measured with the Castaway CTD.

a **b**
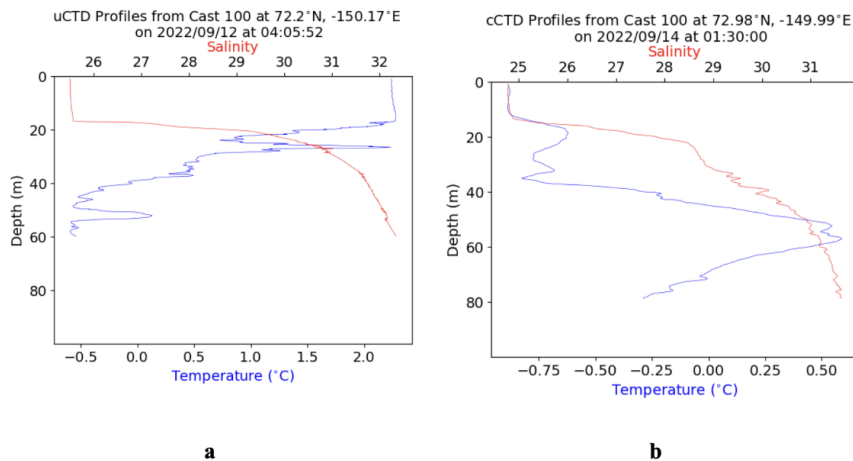
Figure 1~~6~~5. (a) An example uCTD temperature (blue) and salinity (red) from 12 September at 05:40Z at 72.25°N, -150.5°E (b) An example cCTD cast from 14 September at 01:30Z at 72.98°N, -149.99°E. Note the subsurface temperature maxima at ~20 m and at ~55 m in (b). The uCTD cast was taken in open water, whereas the cCTD cast was taken within the ice.

2.1.6 S-band Radar (Drushka, 2023b,c)

The RV *Woldstad* is equipped with a Furuno 2137S-BB S-band marine navigation radar. The ship relied heavily on this radar for navigating through sea ice, particularly during the night and when visibility was low due to fog. X-band radar data have been used in ship-based studies of sea ice (e.g., Lund et al., 2018); S-band radar data have also been used for this purpose (Haykin et al., 1985).

During the SASSIE cruise, screenshots of the ship's S-band radar data were collected by splitting the signal and turning it into a video feed using a screen capture device (Epiphan AV.io HD, Figure 17~~6~~). This video feed was acquired using a command-line video conversion program called "ffmpeg", which saved screenshots as jpegs at a specified time interval: typically, every 60 seconds while the ship was in and around the ice. During JetSSP deployments in the ice, images were acquired every 10 seconds to map the ice evolution in higher resolution. While the ship was in open water for longer than one day, S-band acquisition was paused.

The S-band radar was actively used by the ship's captain and crew for navigation, and the radar settings were adjusted frequently, leading to inconsistencies in the data. Typically, the ship set the radar range to 6 to 12 nm (11 to 22 km) during the daytime and 0.75 to 3 nm (1.4 to 6 km) during the night or in heavy ice concentrations. The captain and mate adjusted the range, heading orientation, and gain as needed to reduce clutter and identify safe routes through the ice. During the night, the radar was set to a lower-brightness night-mode. The radar was switched to standby mode when personnel were on top of the pilot house.

a   b
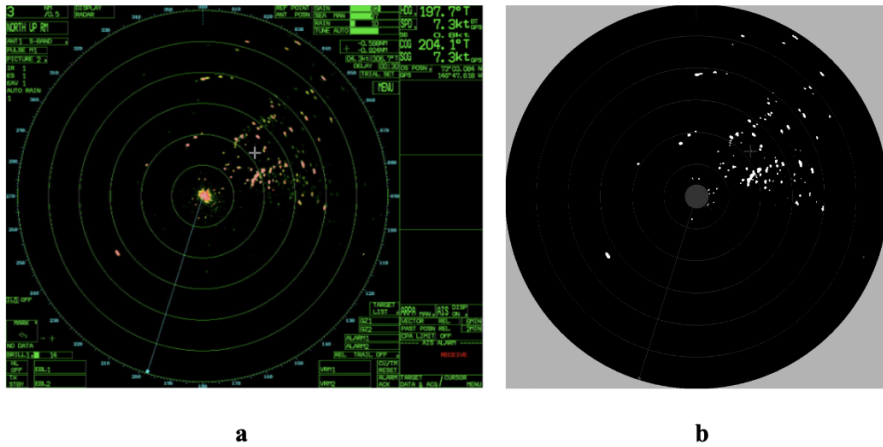
Figure 1~~7~~6. (a) S-band radar snapshot on 19 September 2022 at 00:34Z as the ship was transiting southward out of the ice. Metadata is shown on the image: total range is 3 nm with 0.5 nm per range ring (upper-left of image);~~ north is up in the image~~; image is oriented such that up corresponds to north; ship's heading is shown as the cyan line on the image and the text in the upper-right corner. The presence of ice is indicated by the red-yellow patches in the upper-right quadrant of the range rings. The bright area in the center of the image is sea clutter. (b) The classified image corresponding to Figure 1~~7~~6a, in which each pixel has been classified as "sea ice" (white), "not sea ice" (black), "sea clutter (dark grey), or "no data" (light grey".

Metadata were extracted from the images using MATLAB's computer vision toolbox. The pixels outside of the largest range ring were stripped from each image, and pixels within the range rings were georectified and stored as GeoTIFF images. A data product in which each pixel was classified as sea ice, not sea ice, sea clutter, or not data (e.g., range rings) was also developed (Drushka et al., 2023c). Pixels were classified based on their red, green, and blue (RGB) values: RGB values consistent with yellow to red color ranges were classified as "sea ice" and those consistent with blue-green colors classified as "no data". RGB values were summed as a function of distance from the center of each image: sea clutter appears as a peak in this value. An iterative method was used to identify the distance from center at which sea clutter could no longer be detected; pixels at smaller distances from center were flagged as clutter. The classified image corresponding to Figure 1~~7~~6a is shown in Figure 1~~7~~6b: though the classification is imperfect, it is evident that these data reveal qualitative information about the presence of sea ice around the ship.

2.1.7 Bottle samples for δ18O (Drushka, 2023~~d~~e)

Water samples were collected periodically throughout the cruise for δ18O~~δ18O~~ isotope analysis to help differentiate the sources of the freshwater signals in the SASSIE domain - presumed to be a combination of sea ice meltwater, meteoric water (likely from the Mackenzie River), and Pacific seawater. A total of 45 water samples were collected,

including two duplicates (Figure 1~~8~~7). Water samples were collected ~~either~~ from a GoFlo bottle lowered from a line over the side of the ship to approximately 1 m (N=7 samples), 5 m (N=12), or 30 m (N=1) depth. An RBR~~-~~duet temperature-pressure logger was attached to the GoFlo bottle, providing accurate measurements of the depth and water temperature of the sample. An additional 21 water samples were collected from the Salinity Snake, which pumped water from ~0.05 m depth. Finally, samples were collected during two ice stations on 13 September: tailings from drilling into the sea ice were collected, melted, and stored in sample bottles.

All samples were stored in 20 ml glass scintillation bottles, sealed with parafilm, and later analyzed using a mass spectrometer for δ18O~~δ¹⁸O~~ isotopes at the Oregon State University Stable Isotope Laboratory.

Salinity measurements are needed to interpret δ18O data, and salinity estimates collocated with each water sample are included in the δ18O dataset. Each sample made with the lowered GoFlo bottle was collected within 5 minutes of a uCTD cast at the same location. Water samples made with the Salinity Snake were collocated with Salinity Snake data. Salinity of the sea ice samples estimated as a function of sea ice thickness (measured when the ice samples were made) based on Cox and Weeks (1974).

δ18O values of -5 to -2 mL L-1 were observed throughout the SASSIE domain, except for higher values (-2 to -1.5 mL L-1) in the sea ice samples (Figure 18~~7~~). While these values are generally consistent with previously observed δ18O values observed in Beaufort Sea upper halocline water and sea ice meltwater, and significantly higher than δ18O values of meteoric water (e.g., Lansard et al., 2012), further analysis is needed to quantify the sources of freshwater in the area.
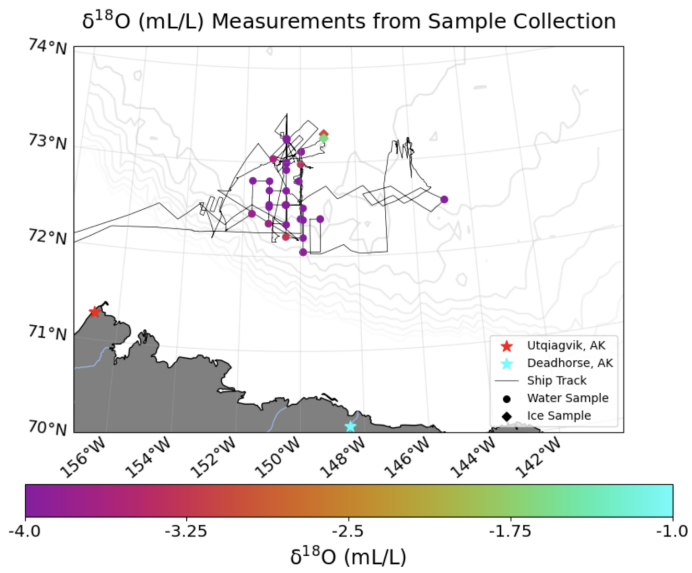
Figure 187. Locations and measurements of the δ18Oδ¹⁸O ratio measurements and the value recorded. Water samples are shown as circles (·) and ice samples are shown as diamonds (♦). The track of the RV *Woldstad* is shown as a black line.

2.2 Piloted & Drifting Platforms

2.2.1 Wave Gliders (Thomson, 2023a)
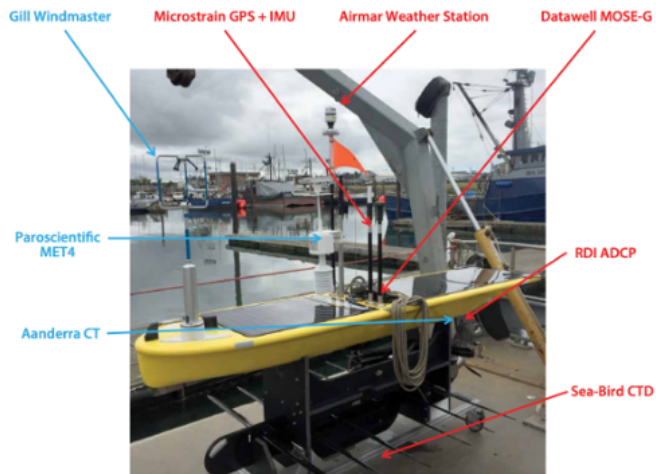
Figure 1~~9~~8. Labeled photo (Thomson and Girton~~et al.~~, 2017) showing the instruments on Wave Glider SV3-153. ~~Photo credit Jim Thomson.~~
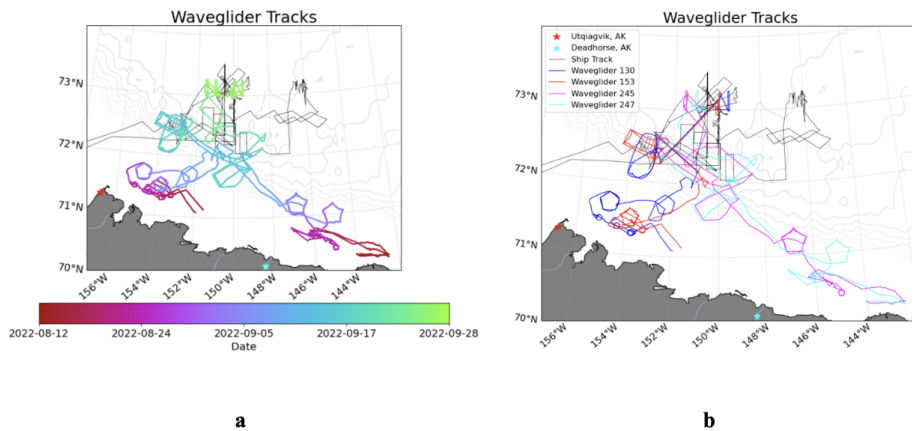
a   b

Figure 2~~0~~19. Paths of the four Wave Gliders throughout the course of the SASSIE campaign, colored by (a) time ~~(a)~~ and (b) Wave Glider number ~~(b)~~. Track of the RV *Woldstad* (black line) and bathymetry contours (gray lines) are also shown for reference.

Four Wave Gliders (model SV3 built by Liquid Robotics, Inc.) from APL-UW~~UW/APL~~ were operated throughout the SASSIE campaign. The Wave Gliders were deployed from the RV *Ukpik* operating out of Prudhoe Bay in early

August. They were recovered for battery charging and redeployed twice from the RV *Woldstad* in September (Table 3), and the final recovery was in late September from the *Woldstad*. Each Wave Glider operated for approximately 50 days and covered almost 1000 nm, often within 10 nm of the sea ice (as determined from the NWS Alaska Sea Ice Program accessed at https://www.weather.gov/afc/ice, an operational product that ingests visible imagery to help include low ice concentration areas).

.

Wave Glider (SV3) numberWave Glider (SV3) number	Deployment dateDeployment location	Deployment locationDeployment date	Recovery DateRecovery Location	Recovery LocationRecovery Date
130130	2022-08-14T20:00:00Z71.08 °N, 151.91 °W	71.08°N, 151.91 °W14-Aug-2022 20:00:00	2022-09-12T18:30:00Z72.66 °N, 152.86°W	72.66°N, 152.86°W12-Sep-2022 18:30:00
	2022-09-12T18:00:00Z72.66 °N, 152.86 °W	72.66°N, 152.86 °W12-Sep-2022 18:00:00	2022-09-25T02:30:00Z73.08 °N, 150.19°W	73.08°N, 150.19°W25-Sep-2022 02:30:00
	2022-09-25T02:00:00Z73.08 °N, 150.19 °W	73.08°N, 150.19 °W25-Sep-2022 02:00:00	2022-09-28T19:30:00Z73.00 °N, 150.19°W	73.00°N, 150.19°W28-Sep-2022 19:30:00
153153	2022-08-14T20:00:00Z71.12° N, 151.54 °W	71.12°N, 151.54 °W14-Aug-2022 20:00:00	2022-09-12T18:30:00Z72.63 °N, 152.80°W	72.63°N, 152.80°W 12-Sep-2022 18:30:00
	2022-09-12T18:00:00Z72.63° N, 152.80 °W	72.63°N, 152.80 °W12-Sep-2022 18:00:00	2022-09-25T02:30:00Z73.06 °N, 150.19°W	73.06°N, 150.19°W25-Sep-2022 02:30:00
	2022-09-25T02:00:00Z73.06° N, 150.19 °W	73.06°N, 150.19 °W25-Sep-2022 02:00:00	2022-09-28T19:30:00Z73.00 °N, 150.42°W	73.00°N, 150.42°W28-Sep-2022 19:30:00
245245	2022-08-12T23:00:00Z70.31° N, 144.04 °W	70.31°N, 144.04 °W12-Aug-2022 23:00:00	2022-09-12T18:30:00Z72.58 °N, 152.66°W	72.58°N, 152.66°W12-Sep-2022 18:30:00
	2022-09-12T18:00:00Z72.59° N, 152.66 °W	72.59°N, 152.66 °W12-Sep-2022 18:00:00	2022-09-21T18:30:00Z72.52 °N, 150.01°W	72.52°N, 150.01°W21-Sep-2022 18:30:00
	2022-09-21T18:30:00Z72.51° N, 150.03 °W	72.51°N, 150.03 °W21-Sep-2022 18:30:00	2022-09-28T19:30:00Z73.00 °N, 150.77°W	73.00°N, 150.77°W28-Sep-2022 19:30:00
247247	2022-08-12T23:00:00Z70.30° N, 143.89 °W	70.30°N, 143.89 °W12-Aug-2022 23:00:00	2022-09-12T18:30:00Z72.55 °N, 152.59°W	72.55°N, 152.59°W12-Sep-2022 18:30:00

2022-09-12T18:00:00Z~~72.55°N, 152.59 °W~~	72.55°N, 152.59 °W~~12-Sep-2022 18:00:00~~	2022-09-26T01:30:00Z~~72.99°N, 150.53°W~~	72.99°N, 150.53°W~~26-Sep-2022 01:30:00~~
2022-09-26T01:00:00Z~~73.00°N, 150.53 °W~~	73.00°N, 150.53 °W~~26-Sep-2022 01:00:00~~	2022-09-28T19:30:00Z~~72.99°N, 150.62°W~~	72.99°N, 150.62°W~~28-Sep-2022 19:30:00~~

Table 3. Deployments of Wave Gliders throughout the SASSIE campaign. ~~Times in UTC.~~

405

Each Wave Glider included a standard package to measure meteorological data (Airmar WX200 sensor), waves (GPSWaves by Thomson et al, 2018), ocean currents (RDI 300 k~~K~~Hz ADCP), near-surface temperature and salinity (Aanderaa CT) and sub-surface temperature and salinity (Seabird GPCTD) (Table 4). Some of these sensors, such as

410 the ADCP and the Airmar, only operated for a fraction of the mission as a battery saving strategy. Salinity measurements from the Aanderaa CT and the Seabird GPCTD sensors agree with a root-mean-square difference of 0.1 (not shown). Two of the W~~w~~ave G~~g~~liders include profiling winches for CTD measurements beneath the sub (8 to 150 m). These prototype systems collected a total of 39 profiles before failing; th~~ose~~at data ar~~e~~is included in the L1 data but did not pass quality control for inclusion in the L2 data.

415

Sensor	Variables Collected	Notes
Airmar WX200 sensor	Air temperature and pressure, wind speed	Only operated for a fraction of the deployment time to conserve battery life.
GPS waves	Wave height, period, and direction	Also, frequency spectra and directional moments
RDI 300 k~~K~~Hz Acoustic Doppler Current Profiler	Ocean current speed and direction	Only operated for a fraction of the deployment time to conserve battery life.
Aanderaa model 4319B CT sensor	Conductivity and temperature at 0.2_5_ m and 1.00 m depth	Some gaps in data due to occasional sensor failure.
Seabird GPCTD	Conductivity, temperature and depth at 54 or 108 m	Only on SV3-130 (54 m) and SV3-153 (108 m)
D2 profiling CTD	Conductivity, temperature, depth up to 150 m per cast (about once per day while operational).	Only equipped on Wave Gliders SV3-245 (31 casts total) and SV3-247 (8 casts total)

Table 4. List of sensors and variables collected by Wave Gliders.

a   b
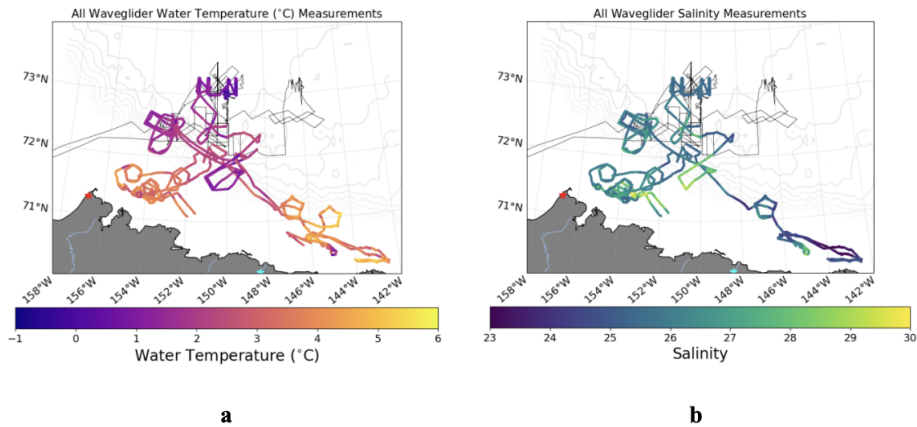
Figure 20. Paths of all four Wave Gliders throughout the course of the SASSIE campaign, colored by (a) water temperature salinity (a) and (b) salinitywater temperature (b) at 0.25 m depth, except in the case of salinity measurements of Wave Glider 153, which were taken at 1 m depth. Track of the RV *Woldstad* (black line) and bathymetry contours (gray lines) are also shown for reference.
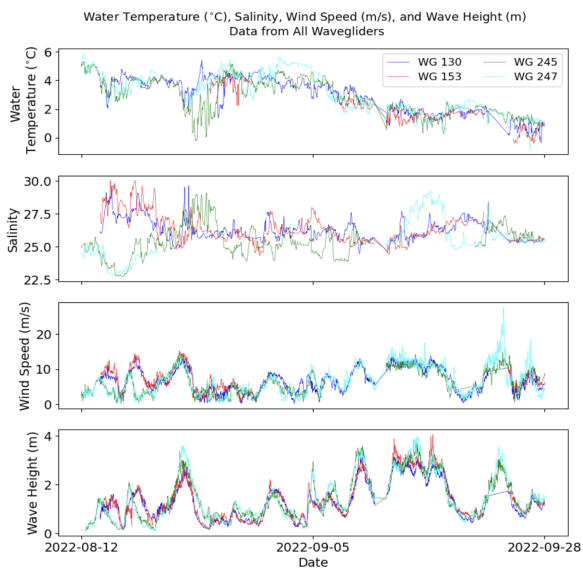
Figure 221. Time series of water temperature, salinity, wind speed, and wave height measurements made by the four Wave Gliders throughout the SASSIE campaign. Temperature and salinity measurements are from 0.25 m depth, except for the salinity measurements from Wave Glider 153 that were made at 1 m depth.

2.2.2 JetSSP (Drushka, 2023ed)

The JetSSP is an autonomous unmanned surface vesselUSV designed to measure salinity gradients in the upper meter of the ocean. The system consists of a 3.1 m long gasoline powered jet-kayak that is controlled using an onboard suite of drone hardware to enable autonomous navigation (Figure 232). Telemetry data is broadcast over a 900 MHz antenna as well as independent AIS and Iridium trackers. The vehicle has fuel capacity to perform 12+ hr autonomous sampling missions traveling at speeds of 4 to 5 kts. A 1 m long keel is bolted to the underside of the vehicle and outfitted with three SBE 49 CTDs that sampled below the water line (Figure 232b).

a   b
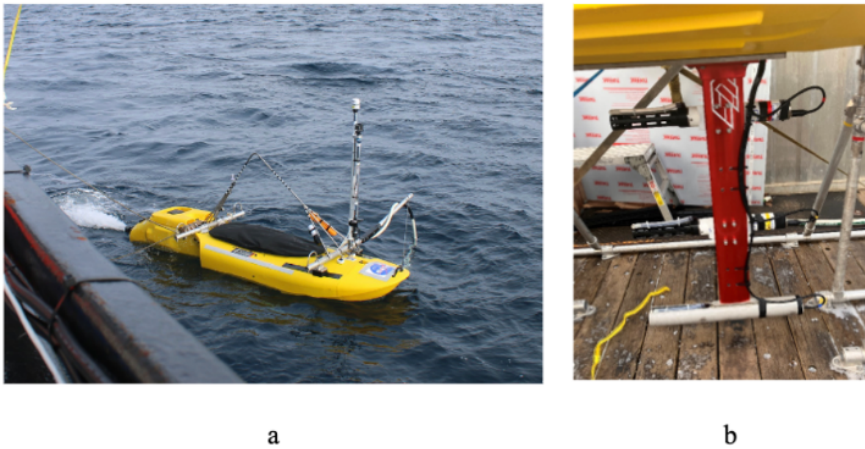
Figure 232. (a) The JetSSP just after deployment. Note the forward meteorology mast and the hose off the port side for the salinity snake. (b) The 1 m-long keel of the JetSSP with three CTDs; the front end of the platform is to the left in the photo. Photo credit Alex de Klerk

In addition, a miniaturized "salinity snake" consisting of a SBE 45 TSG, a positive displacement pump, and a vortex debubbler is mounted internally in order to sample water from a hose dragged at the surface. Using these four instruments JetSSP is able to continuously measure salinity and temperature at nominal depths of 0.05, 0.25, 0.65 and 1.05 m, capturing the very near-surface signature of horizontal and vertical salinity and temperature gradients associated with freshwater layers (Figures 243 and 254). A forward mast with an Airmar 200WX-IPX7 weather station reports air temperature and pressure, and GPS-corrected true wind speed and direction. Data are logged at 6 Hz with a WETLabs DH-4 logger.
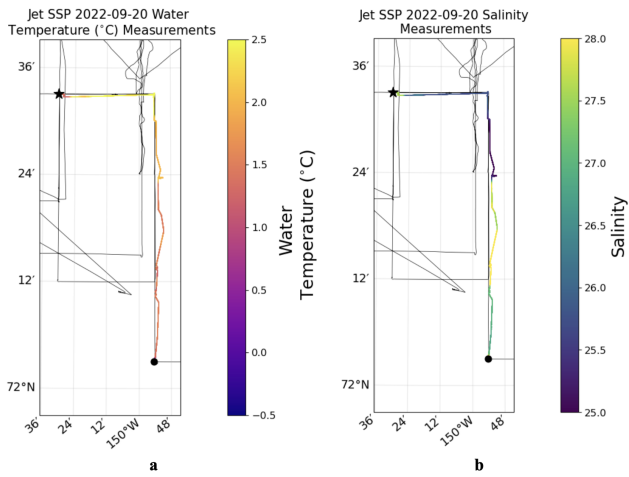
Figure 2~~3~~. Tracks of JetSSP deployment 4 on 09-20-2022 color-coded by (a) temperature ~~(a)~~ and (b) salinity ~~(b)~~ taken at 0.05 m depth. The thin lines show the track of the RV *Woldstad.* Black circle marks initial deployment location and black star marks the recovery.
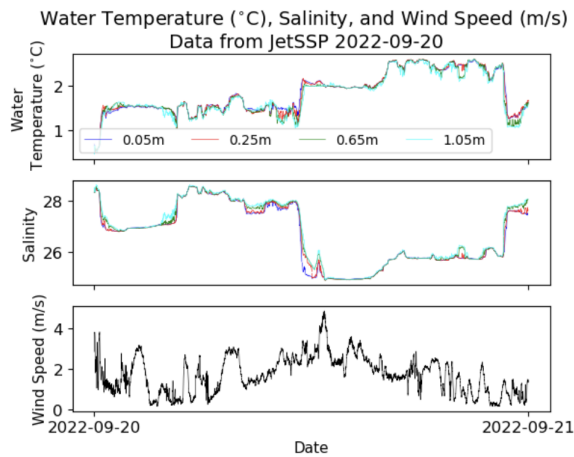
Figure 2~~5~~4. (top) Sea water temperature ~~(top)~~, (middle) salinity ~~(middle)~~, and (bottom) wind speed ~~(bottom)~~ records from Jet-~~ ~~SSP deployment on 20 September.

The JetSSP platform was deployed from the ship and successfully collected data seven times (Table 5, Figure 2~~6~~5). On the eighth ~~and final~~ deployment, the platform was lost.
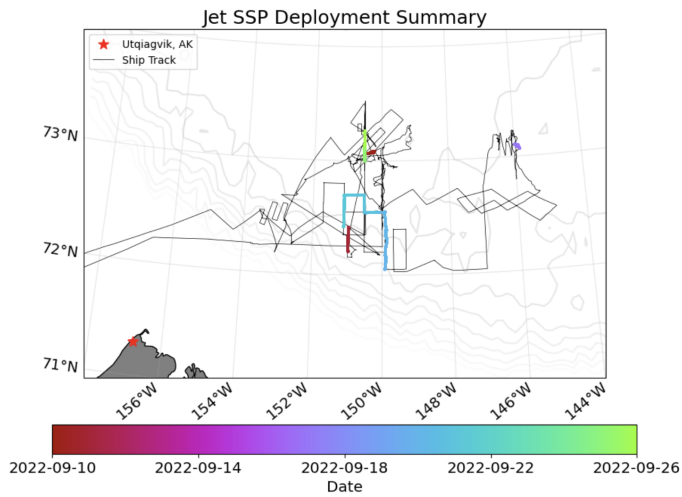
Figure 25. **Paths of Jet SSP deployments throughout the course of the SASSIE campaign, colored by time. Track of the RV *Woldstad* (black line) and bathymetry contours (gray lines) are also shown for reference.**

Deployment number	Deployment date	Deployment Location	Recovery Date	Recovery Location
1	2022-09-10T23:31:00Z	73.07°N, 150.25°W	2022-09-11T02:15:59Z	73.06°N, 150.46°W
2	2022-09-11T19:55:00Z	72.20°N ,150.95°W	2022-09-11T23:03:59Z	72.41°N, 150.95°W
3	2022-09-17T17:34:00Z	73.06°N, 145.84°W	2022-09-17T21:09:58Z	73.09°N, 145.91°W
4	2022-09-20T18:21:00Z	72.05°N, 149.90°W	2022-09-21T03:41:59Z	72.55°N, 150.51°W
5	2022-09-21T17:37:00Z	72.55°N, 150.13°W	2022-09-22T03:59:59Z	72.42°N, 151.10°W
6	2022-09-25T17:09:37Z	73.01°N, 150.50°W	2022-09-26T03:07:49Z	73.24°N, 150.51°W
7	2022-09-26T16:00:00Z	73.11°N, 150.50°W	2022-09-26T19:47:59Z	73.14°N, 150.51°W

Deployment number	Deployment date	Deployment Location	Deployment duration (hours)
1	10 September	73.07°N, 150.25°W	2.8

2	11 September	72.20°N ,150.95°W	3
3	17 September	73.06°N 145.84°W	3.5
4	20 September	72.05°N 149.90°W	9.3
5	21 September	72.55°N 150.13°W	10.5
6	25 September	73.01°N 150.50°W	10
7	26 September	73.11°N 150.50°W	3.8

Table 5. Deployment and recovery dates and, locations and durations for the Jet-SSP. Dates are local time.

460   **2.2.3 SWIFT (Thomson, 2023b)**

Five Surface Wave Instrument Floats with Tracking (SWIFTs; (Thomson 2012) were repeatedly deployed and recovered in the Beaufort Sea during the SASSIE field campaign (Figure 276). SWIFTs are freely drifting buoys that measure waves, winds, temperature, salinity, turbulence, and velocity profiles in a surface-following reference frame (Figure 287).

a   b
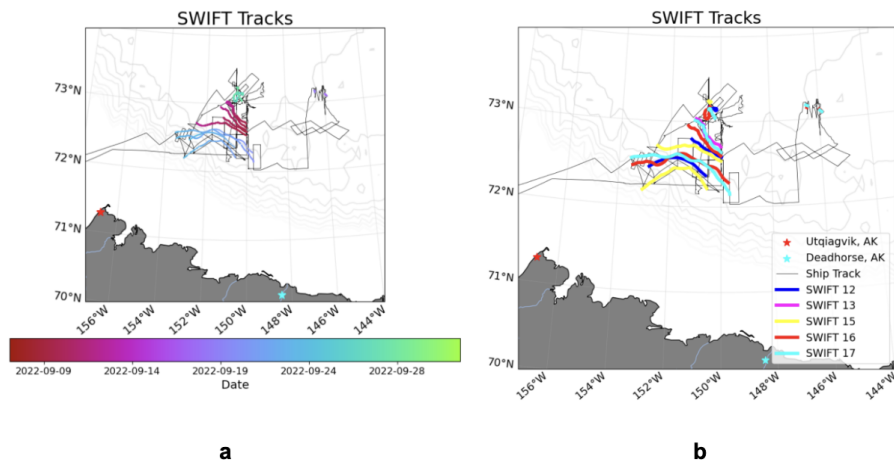
465

 Figure 276. Paths of the five SWIFTs over multiple deployments throughout the course of the SASSIE campaign, colored by time (a) and SWIFT number (b). Track of the RV *Woldstad* (black line) and bathymetry contours (gray lines) are also shown for reference.
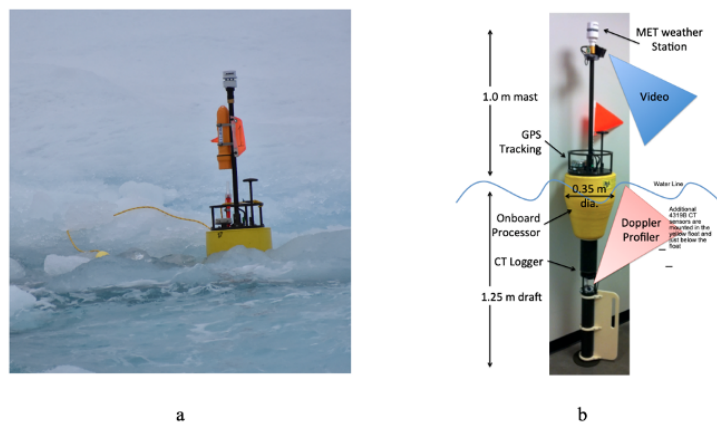
Figure 2~~8~~. (a) A SWIFT floating within slushy ice. Photo credit E J Rainville. **(b)** A SWIFT in the lab with dimensions and notation. Visible in (a) is a small yellow float and line that trails behind the drifting SWIFT to make it easier to recover with a grappling hook.

For SASSIE, additional conductivity and temperature (CT) sensors (Aanderaa model 4319B) were added to most buoys (Figure 2~~9~~8b). The configurations varied from a full suite of three CT sensors at depths of 0.2, 0.6, and 1.2 m on some buoys, to a single CT sensor at 0.6 m on other buoys. These configurations varied between deployments, as repairs and replacements required. Buoys without three CTs included a camera with images of surface conditions (including sea ice, Figure 2~~9~~8a). The reported salinity values are determined onboard each CT sensor using a factory calibration. The uppermost CT (at 0.2 m depth) on each SWIFT has a salinity offset of almost 1 that is caused by proximity of the inductive core to the buoy floatation collar: this offset was removed from the final dataset. During high sea states, the uppermost CT is also contaminated by bubbles.

The deployments were organized into a series of plays, coordinated with other drifting buoys, floats, and shipboard sampling by the RV *Woldstad*. The SWIFT collections and conditions are summarized Table 6. Data collection during Play 1 employed five bursts of raw data per hour. Data collection during all other plays used a single burst (512 s) of raw data per hour, to conserve battery power. The L2 data are statistical products for each burst that are calculated from the raw data (collected at 4 Hz).

During several plays, a line of SWIFTs was deployed across a lateral surface salinity gradient to capture the evolution of the gradient over time and space (~~e.g.,~~ Figure 2~~9~~8). For instance, during play 1, five SWIFTs were deployed along a 18 km meridional line and allowed to drift for ~ 2 days. During play 4, four SWIFTs were deployed across a 40 km long line.

a   b
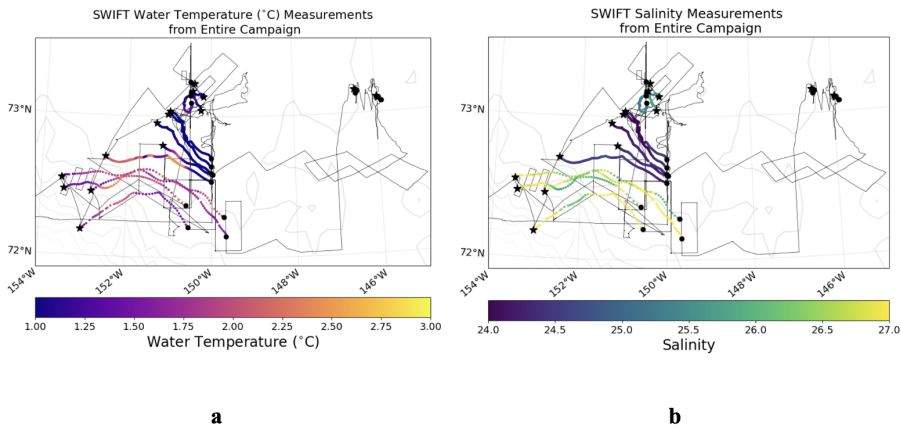
Figure 2~~9~~8. (a) Temperature~~Salinity (a)~~ and ~~temperature~~ (b) salinity measurements taken by SWIFTs throughout the SASSIE campaign. Track of the RV *Woldstad* (black lines) and bathymetry data (gray lines) shown for reference. Deployment locations are shown as a circle (•) and recovery locations are shown as a start (★).

SWIFT identifier	Play number	Deployment date	Deployment location	Recovery Date	Recovery Location
12	1	2022-09-09T21:24:00Z	72.5860°N, 149.9649°W	2022-09-11T07:00:00Z	72.7944°N, 151.1581°W
	4	2022-09-22T10:00:42Z	72.3682°N, 150.5954°W	2022-09-23T23:03:20Z	72.4583°N, 152.8195°W
	5	2022-09-25T22:04:29Z	73.1734°N, 150.4843°W	2022-09-28T01:01:30Z	73.1387°N, 150.1784°W
13	1	2022-09-10T03:36:00Z	72.7033°N, 149.9960°W	2022-09-13T03:36:00Z	73.0359°N, 150.9906°W
15	1	2022-09-09T22:12:00Z	72.5380°N, 149.9941°W	2022-09-12T20:00:00Z	72.7068°N, 152.5120°W
	4	2022-09-21T10:10:16Z	72.2162°N, 150.5449°W	2022-09-23T18:10:52Z	72.1854°N, 153.0444°W
	5	2022-09-28T00:10:55Z	73.2440°N, 150.4968°W	2022-09-29T01:11:56Z	73.2350°N, 150.4047°W
16	1	2022-09-10T02:10:00Z	72.5973°N, 149.9980°W	2022-09-12T18:58:00Z	72.9517°N, 51.2988°W

495

		3a	2022-09-17T17:44:17Z	73.0772°N, 145.8576°W	2022-09-17T21:46:20Z	73.1112°N, 145.9708°W
		3b	2022-09-18T18:44:05Z	73.1378°N, 146.4767°W	2022-09-18T20:49:11Z	73.1592°N, 146.4796°W
		4	2022-09-20T06:44:35Z	72.2864°N, 149.7039°W	2022-09-23T15:45:55Z	72.4680°N, 153.4623°W
		5	2022-09-25T23:10:42Z	73.0961°N, 150.4869°W	2022-09-29T00:11:58Z	73.1788°N, 150.443°W
17		1	2022-09-10T02:48:00Z	72.6435°N, 149.9938°W	2022-09-13T03:12:00Z	73.0146°N, 151.0330°W
		3a	2022-09-17T18:10:20Z	73.0777°N, 145.8670°W	2022-09-17T22:12:07Z	73.0993°N, 145.9544°W
		3b	2022-09-18T18:12:06Z	73.1567°N, 146.4397°W	2022-09-18T20:14:47Z	73.1679°N, 146.5071°W
		4	2022-09-20T04:13:30Z	72.1495°N, 149.6523°W	2022-09-23T14:12:21Z	72.5492°N, 153.5298°W
		5	2022-09-26T20:13:38Z	73.1458°N, 150.4996°W	2022-09-28T23:11:17Z	73.0436°N, 150.2418°W

Table 6. A list of deployment dates and locations for SWIFT buoys.

2.2.4 HydroBuoys (Steele, 2023)

500   The SASSIE HydroBuoys were designed to measure both surface hydrography (i.e., SST and SSS) as well as subsurface temperature and salinity to provide thermal and haline stratification. They were deployed by the RV Woldstad during the cruise~~during the September 2022 SASSIE cruise~~ and not recovered, thus providing persistent observations through the fall and even into the winter.

505   These buoys were based on surface-drifting buoys deployed in the Arctic Seas by the UpTempO project (http://psc.apl.washington.edu/UpTempO/; Castro et al., 2016, Banzon et al., 2020), which generally focuses on temperature observations only. For SASSIE, conductivity sensors were added to measure salinity. A variety of sensor configurations were used on a total of 11 buoys deployed during SASSIE, from surface-only temperature and salinity to a heavily instrumented string of sensors extending down to 60 m depth (Figure 30~~29~~; Table 7). All buoys provide
510   data at 10-minute intervals. The buoys generally drift with the surface currents (or ice in the winter); six~~several~~ were equipped with a drogue consisting of "holey sock" fabric cylinders that are 1 m in diameter and 6 m in length, centered at 15 m depth.
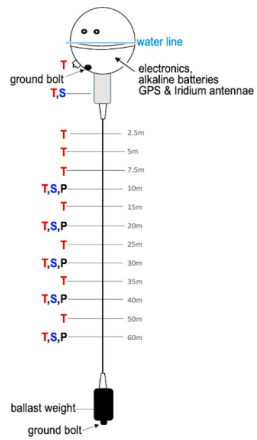
Figure 3029. Schematic of SASSIE HydroBuoy 009, with sensors measuring ocean temperature (T), conductivity from which salinity is derived (S), and pressure (P). Other buoys had as many or fewer sensors (Table 7). This buoy did not include a drogue, whereas some others did.

Drifter number	Deployment Time	Deployment Location	Temperature Data Depths (m)	Salinity Data Depths (m)	Pressure Data Depths (m)	Drogue
HydroBuoy 001	2022-09-09T00:04:00Z	72.2515°N, 151.3799°W	0.14, 0.44, 5	0.38, 5	5	yes
HydroBuoy 002	2022-09-09T00:16:00Z	72.2516 °N, 151.3828°W	0.14, 0.44	0.38	N/A	no
HydroBuoy 003	2022-09-10T00:00:00Z	72.4064°N, 150.0226°W	0.25, 2.5, 5, 7.5, 10, 15, 20, 25, 30, 35, 40, 50, 60	10, 20, 30, 40, 60	10, 20, 30, 40, 60	no
HydroBuoy 004	2022-09-11T18:10:00Z	73.0742°N, 150.2654°W	0.14, 0.44, 5	0.38, 5	5	yes
HydroBuoy 005	2022-09-13T18:40:00Z	73.2626°N, 149.1335°W	0.25, 2.5, 5, 7.5, 10, 15, 20, 25, 30, 35, 40, 50, 60	10, 20, 30, 40, 60	10, 20, 30, 40, 60	no
HydroBuoy 006	2022-09-15T22:40:00Z	72.6197°N, 145.3558°W	0.14, 0.44	0.38	N/A	yes
HydroBuoy 007	2022-09-17T18:00:00Z	72.8467°N, 146.0011°W	0.14, 0.44	0.38	N/A	no
HydroBuoy 008	2022-09-20T02:10:00Z	72.0334°N, 149.2567°W	0.14, 5	5	5	yes
HydroBuoy 009	2022-09-20T07:00:00Z	72.0330°N, 149.2609°W	0.25, 0.57, 2.5, 5, 7.5, 10, 15, 20, 25, 30, 35, 40, 50, 60	0.51, 10, 20, 30, 40, 60	10, 20, 40, 60	no

Inserted Cells

HydroBuoy 010	2022-09-25T17:10:00Z	73.0317°N, 150.8290°W	0.14, 5	5	5	yes
HydroBuoy 011	2022-09-25T20:50:00Z	73.0316°N, 150.8291°W	0.14, 5	5	5	yes

Table 7 Deployment location, time, and nominal depths (i.e., when the sensor string is hanging vertically) of available temperature, salinity, and pressure data of SASSIE HydroBuoys, as well as whether the buoy had a drogue. As of March 2024, HydroBuoys 002, 007, 008, and 009 were still recording.

520 Buoys with subsurface sensor strings also had ocean pressure sensors to determine changes in hydrography sensor depths owing to several reasons, i.e., (1) sensor string uplift owing to wind or ice pushing the surface hull, which makes the trailing sensor string rise up in the water column (this is very common), (2) sea ice ridging, which pulls up the sensor string into the ice (this often happens during winter), and (3) dragging on the ocean bottom (this generally happens when a buoy transits over the continental shelf, which did not happen during SASSIE). All buoys generally

525 drifted west, northwest, and north after deployment (Figure 310). All buoys performed well until they encountered ice (generally in late September through early December 2022), at which time communications stopped for many but not all buoys. As of September 2023, 4 buoys were still reporting, all of which had drifted northward to ~ 86N, 135W over the Alpha Ridge. Four buoys were still reporting sea surface temperature (SST), three were reporting sea surface salinity (SSS), and one was reporting surface and subsurface temperature and salinity.
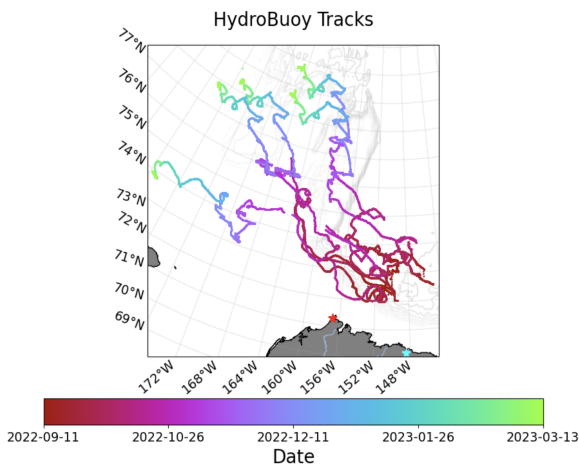
530

Figure 310. Paths of the SASSIE HydroBuoys throughout the SASSIE campaign and beyond. Shown are drift tracks from deployment in September 2022 through March 2023.

An example of buoy data is provided in Figure 321. The ocean temperature data shows gradual cooling at the surface, and warm intrusions at depth that are likely summer Pacific Water entering the southern Beaufort Sea from the north-

535 eastern Chukchi Sea. The ocean salinity data shows declining stratification in the upper water column as fresh meltwater is mixed downward and salinified via ice growth and brine rejection.
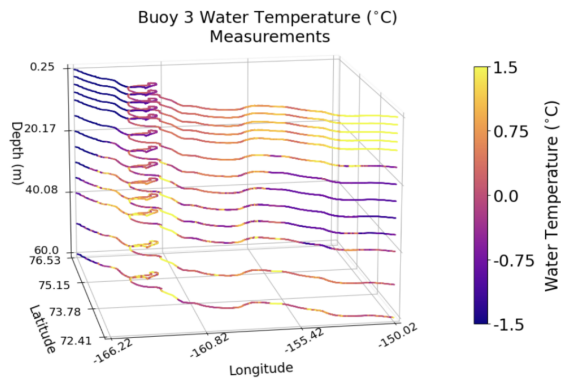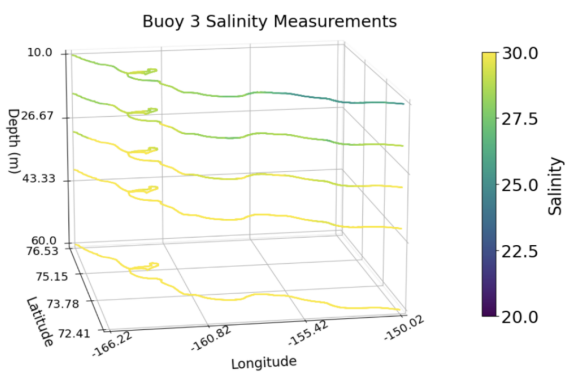
Figure 3~~2~~1. Water temperature and salinity measurements by HydroBuoy 3.

2.2.5 Under-Ice Float (Shcherbina, 2023)

A UIF is a heavily instrumented autonomous profiling vehicle based on the Mixed-layer Lagrangian float design (e.g., D'Asaro, 2003). The SASSIE UIF was outfitted with two pumped Seabird SBE 41CP CTDs mounted on the top and the bottom of the float, a narrow-beam upward-looking Valeport VA500 sonar, and an upward-looking camera for ice imaging (Figure 3~~3~~2).

545 **Figure 32. The UIF on the deck of the Woldstad before deployment. The float is about 2 m tall from the deck to the top of the antennas. Note CTDs at top and bottom of the float, upward-looking camera mounted near the top of the float body on the left, and an ice-profiling sonar attached to the right-hand side. Photo credit Jim Thomson.**

The UIF was deployed from RV *Woldstad* on 10 September 2022 at 20:05 UTC at 73.12°N, 149.93°W within the marginal ice zone (Figure 33). During its deployment, the float made frequent vertical profiles, surfacing when 550 possible (i.e., when the sonar detected open water) to telemeter data. The last data transmission occurred on 23 October 2022.
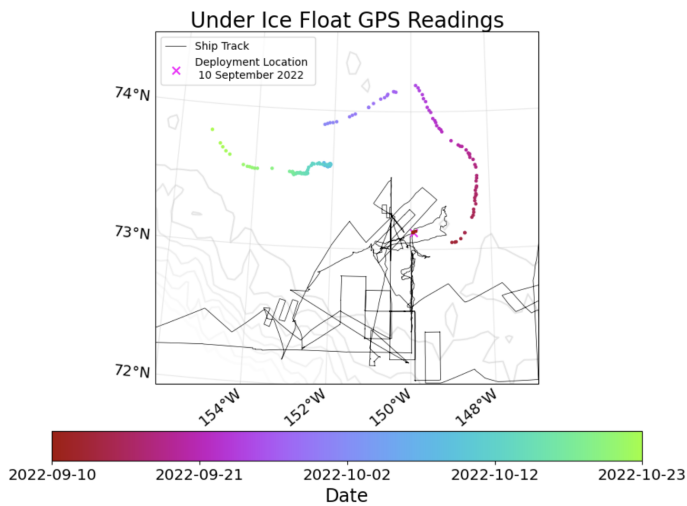
Figure 33. GPS Readings from the Under Ice Float colored according to date. The gaps in the record indicate the periods of heavy ice that prevented float surfacing. Black line denotes ship track.

555 UIF profiling was focusing on the upper 40-50 m of the water column to resolve the evolution of the cold and fresh mixed layer in the later stages of summer ice melt and the transition to freeze-up (Figure 3~~5~~4). Particular attention was paid to the upper meters under the ice or open water, where vertical CTD resolution down to 1 cm was achieved through reduced profiling speed and increased sampling rate (Figure 3~~6~~5). The frequency of the profiles varied through the course of the mission, but it was typically between 12 and 18 profiles per day (15 profiles/day on average).

560 Periodically, the UIF spent time hovering 10-15 m below the surface, utilizing its sonar and camera to survey the ice topography and capture photos (Figure 3~~7~~6).

The UIF CTD records (Figures 3~~5~~4-3~~6~~5) show a general increase in salinity, decrease in temperature, and deepening of the mixed layer in September-October. These changes were due to entrainment of saltier pycnocline water accompanied by surface heat loss. Advective changes in the water mass structure were also evident below 30m (within

565 the pycnocline). Until September 30, mixed layer temperature stayed >0.1°C above the freezing point. At that time, the ice cover remained fragmented and consisted of old brash ice (Figure 3~~7~~6a). Even though the temperature approached freezing by October, new ice formation was intermittent. Calm weather periods allowed periodic formation of pancake (Figure 3~~7~~6a) and nilas ice. These new ice formation events were interspersed with prolonged

570 periods of open water and rough seas. Ice formation intensified and started to show signs of consolidation in the second half of October.

a   b
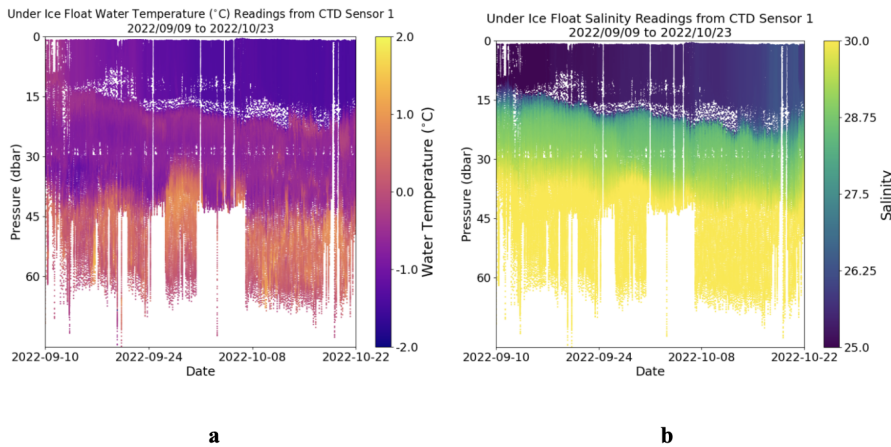
Figure 3~~5~~4. 2D scatterplots of (a) ~~water temperature (a)~~ water temperature and (b) salinity measurements ~~(b) readings~~ from UIF CTD sensor 1 (at the bottom of the UIF; Figure 3~~3~~2) throughout its deployment.

a   b
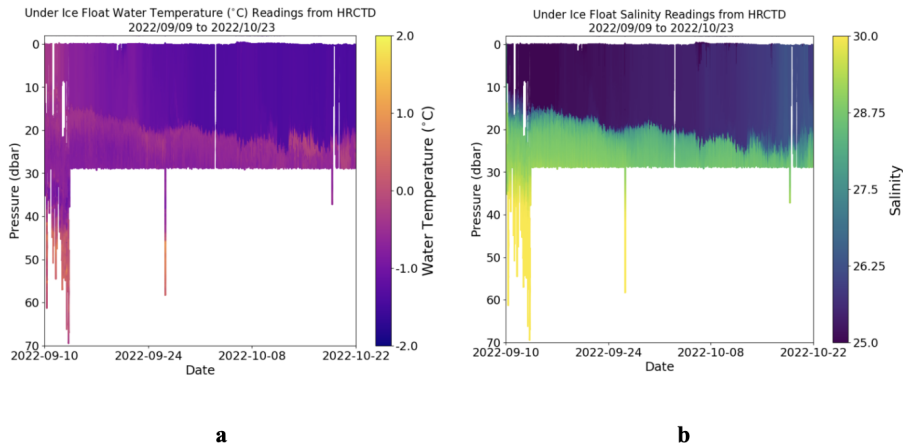
Figure 3~~6~~5. 2D scatterplots of (a) water temperature ~~(a)~~ and (b) salinity measurements~~(b) readings~~ from the UIF high resolution CTD sensor throughout its deployment. The high resolution CTD is seen attached to the top of the float in Figure 3~~3~~2. Note the different color scale and vertical axes between this and the previous figure.

a   b
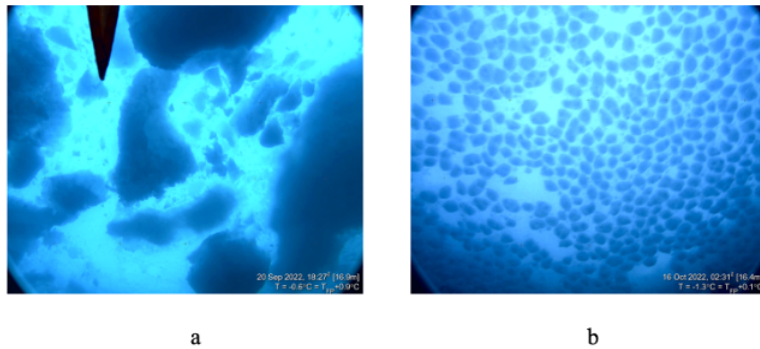
Figure 3~~7~~6. Examples of UIF ice imagery. (~~(~~a) Broken old ice (brash) commonly observed during the first half of the mission. (b) New pancake ice formation observed periodically during the freeze-up. Images are annotated in the lower-right corner with the date, time, UIF depth at that time, observed temperature and its departure from the freezing point (T$_{FP}$). The black shape visible in (a) is the UIF flag.

2.2.7 ALTO and ALAMO Floats (Jayne and Steele, 2023)

 Seven profiling floats (Table 8) manufactured by MRV systems were deployed during SASSIE. These floats provide autonomous profiles of ocean temperature and salinity and were set to sample over the upper 100 m. They thus provide information about SST, SSS, and thermal and haline stratification. The floats profile vertically by changing their

buoyancy, and drift laterally with the local currents. Since the floats were sampling rapidly (multiple profiles per day) over the upper 100 m, their drift is a complex integration of upper ocean current speed and direction.

Float number	Deployment location	Deployment date	Final transmission of 2022
11131 - ALTO	72.25 N, 153.04 W	8 September 2022	10 October
11132 - ALTO	72.25 N, 150.00 W	8 September 2022	14 October
11133 - ALTO	72.25 N, 154.95 W	8 September 2022	14 October
11136 - ALTO	72.25 N, 151.51 W	8 September 2022	24 October
9097 - ALAMO	72.5 N, 145.0 W	15 September 2022	12 October
9101 - ALAMO	72.0 N, 149.5 W	19 September 2022	4 October
9098 - ALAMO	73.12 N, 150.5 W	25 September 2022	12 October

Float number	Deployment date	Deployment location	Final transmission of 2022 Date	Final transmission of 2022 Location
11131 - ALTO	2022-09-08T20:39:00Z	72.2488°N, 153.0426°W	2022-10-14T18:39:00Z	71.9142°N, 152.1613°W
11132 - ALTO	2022-09-09T03:33:00Z	72.2531°N, 150.0152°W	2022-10-14T02:56:00Z	72.6591°N, 154.0011°W
11133 - ALTO	2022-09-08T14:40:00Z	72.2521°N, 155.0015°W	2022-10-14T08:23:00Z	72.5423°N, 155.5976°W
11136 - ALTO	2022-09-09T00:15:00Z	72.2474°N, 151.5357°W	2022-10-14T15:30:00Z	72.4317°N, 152.4742°W
9097 - ALAMO	2022-09-18T16:35:00Z	72.6310°N, 145.6787°W	2022-10-12T01:11:00Z	73.0563°N, 146.8655°W
9101 - ALAMO	2022-09-20T02:22:00Z	72.0383°N, 149.6530°W	2022-10-03T23:19:00Z	72.8990°N, 153.1992°W
9098 - ALAMO	2022-09-25T18:58:00Z	73.1227°N, 150.4935°W	2022-10-12T05:54:00Z	73.7369°N, 147.4949°W

Table 8. Deployment Dates and locations of the ALTO and ALAMO floats. Three additional ALAMO floats were deployed (two on 9 September 2022 and one on 10 September 2022) but did not collect any data.

595 Four of the seven working floats were relatively larger (133 cm long, 16.5 cm, 19.2 kg) ALTO floats (Figure 3~~8~~7), and three were relatively smaller (91 cm long, 12.2 cm diameter, 8.4 kg) ALAMO floats. All floats stopped reporting owing to advancing ice by late September through October 2022 (Figure 3~~9~~8). The ALTO floats included an "ice avoidance" algorithm (e.g., Wong et al., 2020) with the goal of surviving winter. Unfortunately, none of these floats reported in summer 2023. The ALAMO floats did not include this feature to maximize data collection during freeze-600 up.

Figure 3~~8~~7. An ALTO float waiting to be deployed.
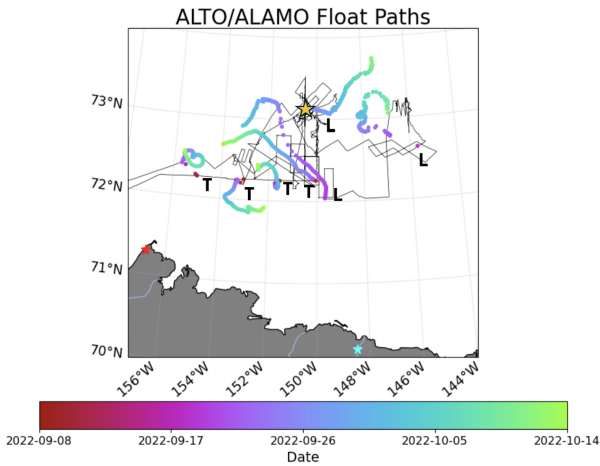
Figure 3~~9~~8. Paths of the ALTO (designated "T") and ALAMO (designated "L") floats throughout the field campaign

605   **colored by date. The path of float 9098 (measurements shown in Figure 40) is marked by an orange star (★).**

An example of float data is provided in Figure 40~~39~~. A clear signal of subsurface warm layers is evident, especially to the southeast at the start of the drift where warm summer Pacific Water is likely entering the Beaufort Sea from the northeastern Chukchi Sea. The data show a rather complex temperature profile that might also include warming from local radiative fluxes (i.e., a Near-Surface Temperature Maximum) which will be investigated using full hydrographic

610   and meteorological analyses.
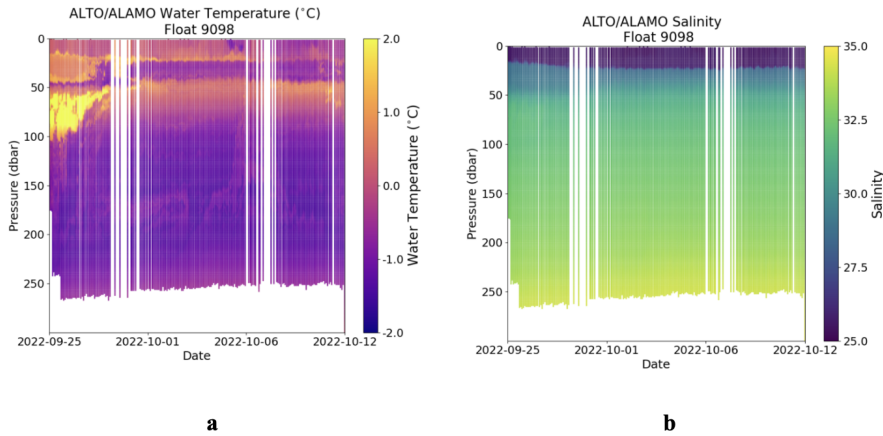
Figure 40~~39~~. Temperature (a) and ~~s~~Salinity (b) measurements~~readings~~ from ALAMO float 9098.

2.3 PALS Aircraft
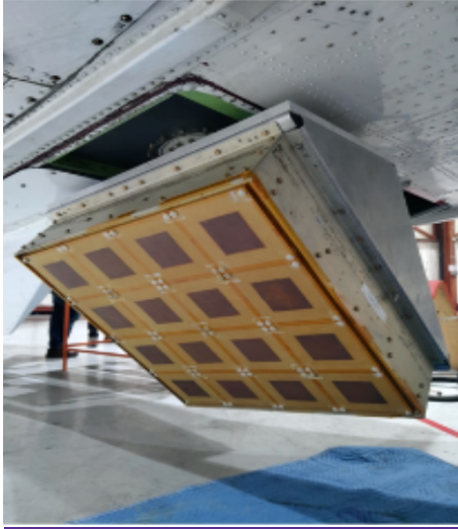
Figure 4~~10~~. PALS patch array antenna installed underneath the DC3-T Basler (BT-67) aircraft. The antenna is mechanically rotated 360 degrees via a scanner motor (not seen) and covered with a radome before flight operations.

To link in situ SSS measurements to SSS patterns across broader spatial scales, airborne measurements of SSS were made with the JPL Passive/Active L-band System (PALS) microwave radiometer (Wilson et al., 2001a,b; Yueh and Chaubell, 2011). The aircraft measurements provided broad-scale context and enabled quantification of SSS and SST, their horizontal gradients, and sea ice signals. PALS measures at the same L-band frequencies as the NASA Soil Moisture Active Passive (SMAP) satellite instrument, with significantly increased spatial resolution and accuracy over shorter timescales. PALS measures at 1.4 GHz with 24 MHz bandwidth and has the capability of measuring at 1.2 GHz with an 80 MHz bandwidth. The combination of these two frequencies significantly increases the sensitivity to salinity in cold waters. PALS can provide 300 m to 1500 m horizontal resolution when flying at altitudes of 1 to 3 km. The airborne PALS radiometer has significantly smaller measurement noise compared to satellite radiometers because airborne platforms have far longer scene integration times and therefore a greater reduction of uncorrelated measurement errors.

After averaging, PALS can theoretically measure SSS in cold waters (SST < 5°C) with 0.2-0.25 resolution over 1 km horizontal scales. During SASSIE, the instrument suite also included a compact wideband (750 MHz) C- and X-band radiometer to measure SST and ocean wind speed, respectively, at approximately 0.3 K and 1 m s^{-1} resolution. The PALS instrument also has an on-board combined infrared (IR) and visible imaging camera that covers a 45-degree swath. The IR camera provides radiometric temperatures for each point at~~on~~ 1.56 m x 1.95 m resolution per acquisition with <50 mK sensitivity when flying at an altitude of 1 km; the visible camera has 0.25 m x 0.33 m resolution when flying at an altitude of 1 km. For surveys over partial ice cover, the visible and IR imagery provide high-resolution

estimates of ice concentration for comparison with and validation of satelliteSAR-derived ice concentration. The combination of the embedded GPS and IMU modules with the dual visible and thermal camera capability provides time-stamped and geolocated radiometric measurements that can be synchronized with the PALS radiometer measurements.

640

PALS was installed in a Basler DC3-T aircraft operated by Kenn Borek Air Limited, a Canadian operator. Five PALS flights were made during SASSIE (Table 9): flights 1 and 3 were over the RV *Woldstad* and flights 2, 4 and 5 were over Wave Gliders (Figure 421).

645

Flight number	Date (2022)
1	11 September
2	14 September
3	16 September
4	17 September
5	18 September

Table 9. Dates of PALS flights.
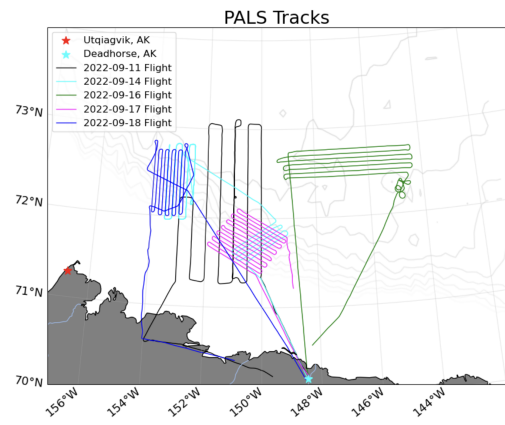
Figure 421. Map of the PALS flights. Different colors indicate different flights (Table 9) as shown in the legend at top left. Thin gray lines show bathymetry contours.

650   The PALS airborne measurement data processing consists of converting measured uncalibrated counts to polarized microwave brightness temperature values at 1.2 and 1.4 GHz, and ultimatelywhichthat eventually gets converting thoseed to SSS.

The initial calibration process from uncalibrated measured counts to brightness temperature (Tb) utilizes internal
calibration sources present within the PALS radiometer (noise-diode and reference load) that provide instantaneous
gain and offset calibration coefficients. On-board temperature sensors allow constant tracking of the instrument
temperature variations as the aircraft changes altitudes and outside temperature varies. PALS calibration also takes
into account any potential scan dependent variations within the data observed from sources such as the internal scan
motor, or the external radome etc. Another key data processing step is detecting and excising radio frequency
interference (RFI) from the Tb measurements. During SASSIE flights, 1.2 GHz passive microwave data saw extreme
RFI corruption, making the data almost unusable. The 1.41.4 GHz radiometer data though waweres relatively free of
RFIclean.

Airborne Tb measurements at 1.4 GHz, see contributions from direct and reflected solar and galactic reflection, rain,
RFI, SSS, SST, and ocean wind vectors or sea surface roughness. In order to derive salinity from brightness
temperature, these other parameters need to be corrected for or removed. AtAdditionally, at a coldat cold SST of less
than 10°C, the sensitivity of brightness temperature to salinity is nearly 3 times less than at tropical temperatures.
SASSIE flew in rain-free conditions and took advantage of the 360-degree scan to correct for wind direction signatures
and potential solar or galactic intrusions within the data. Although there wasSASSIE flew an on-board IR sensor to
measurefor SST, but due to mostly cloudy conditions the IR data were contaminated the processing PALS data
reliedhad to rely on ancillary SST values from satellite productss. Wind speed and resulting white-cap foam on the
ocean surface is the most difficult contributor to correct. We use ancillary data such as ASCAT wind vectors as well
as on-board measurements from a C/X band radiometer to derive relative wind speed trends observed during flight
lines. Tb to SSS retrieval is done using the Klein-Swift model for the Dielectric Constant of Sea Water, though other
models such as Meissner-Wentz and GW-model were also tested. The absolute value in all models is slightly different
at cold waters, but the relative variation of salinity during flight lines is similar. We anchor derived SSS absolute
values to "ground-truth" data obtained from the Wwave G gliderassets. At the time of publication, PALS data wereare
still undergoing processing.

3. Plays

The SASSIE cruise revolved around five major "plays" (Table 10), each of which was essentially a mini-experiment
that targeted a particular region, feature, or set of conditions using a tailored sampling strategy and suite of platforms.
The shipboard and aircraft teams determined the location and strategy for each play based on local conditions such as
weather, sea ice, presence of salinity or temperature gradients, as well as relevance to the SASSIE objectives.

Play #	Description	Start date (2022)	End date (2022)
1	Marginal ice zone survey	8 September	13 September

2	Open water survey	14 September	16 September
3	Ice survey	16 September	18 September
4	Drifter-following boxes	19 September	23 September
5	Transects across ice-open water transition	25 September	29 September

685 **Table 10. Summary of SASSIE plays.**

3.1 Play #1: Marginal ice zone survey

Play 1 began as RV *Woldstad* entered the MIZ on 8 September, deploying five ALTO/ALAMO profiling floats, five HydroBuoys, and five SWIFTs during the following days to capture the transition between open ocean and moderate sea ice cover (Figure 4~~3~~2). The ship focused primarily on the sea ice covered waters north of around 72°30'N, while

690 Wave Gliders and the aircraft captured open waters to the south. As the ship navigated through the heaviest ice cover of the expedition (estimated to be >60% ice cover), the UIF was deployed, and water samples were collected at two ice stations to provide end-members for $\delta18O$~~$\delta18O$~~ isotope analysis. Key observations included horizontal surface salinity differences~~gradients~~ of 2 to 3 from open water to ice, with strong surface salinity variability south of the ice edge and homogeneous salinities within ice-covered waters (Figure 4~~3~~3).

695
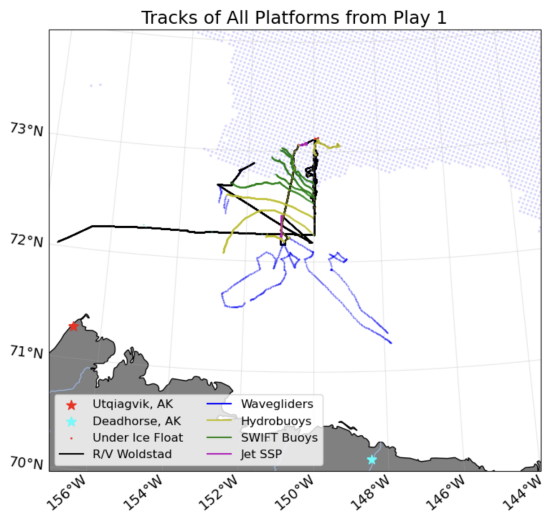
Figure 4~~3~~2. A map showing the tracks of all six platforms during Play 1. Blue stippling indicates an ice concentration greater than 0%~~the presence of ice~~ on 11 September 2022 as determined from the MASIE-NH ice product.

a   b
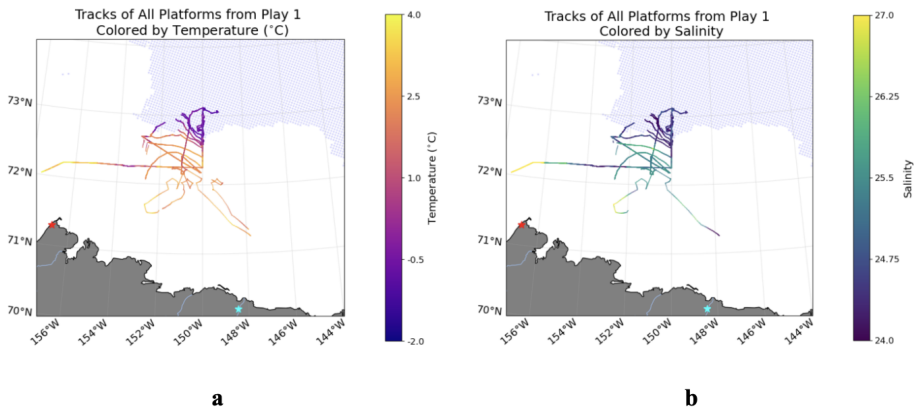
700   **Figure 4~~3~~. (a) Temperature ~~(a)~~ and (b) salinity ~~(b)~~ recorded closest to the sea surface by each asset ~~(except UIF)~~ during Play 1 (except t. The UIF~~under-ice float has been excluded~~ because it does not consistently make measurements near the sea surface). Blue stippling indicates an ice concentration greater than 0% on 11 September 2022, as determined from the MASIE-NH ice product.**

~~Blue stippling indicates the presence of ice on 11 September 2022, as determined from the MASIE-NH ice product.~~

705   **3.2 Play #2: Open water survey**

During Play 2, the ship surveyed south of the ice edge between 150°W and 145°W, forming a zig-zag pattern to maximize sampling of horizontal variability (Figures 4~~5~~4 and 4~~6~~5). Winds and sea state were high, so profiling with the uCTD and JetSSP was limited. Conditions for flying were excellent, and the aircraft performed two surveys: one day over the Wave Gliders southwest of the ship in open water and another day in long east-west transects over the

710   ship. The ship reached its easternmost point during this play.
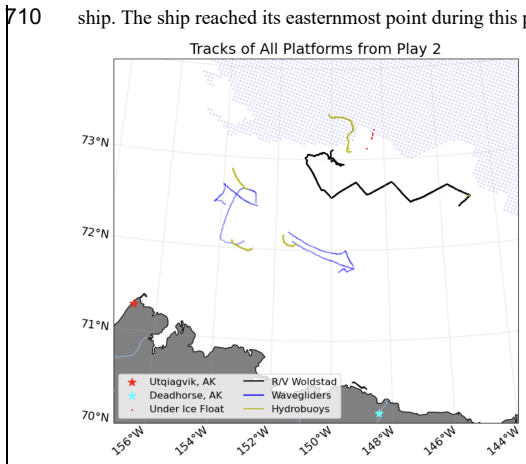
Figure 4~~4~~5. A map showing the tracks of all six platforms deployed during Play 2. Blue stippling indicates _an ice concentration greater than 0%_ ~~the presence of ice~~ on 15 September 2022 as determined from the MASIE-NH ice product.

a   **b**
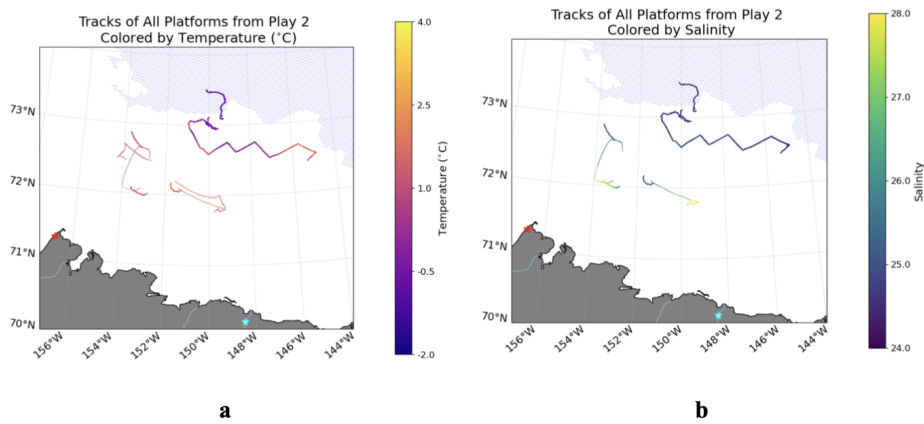
715   **Figure 4~~6~~5. _(a)_ Temperature ~~(a)~~ and _(b)_ s~~S~~alinity ~~(b)~~ recorded closest to the sea surface by each asset _(except UIF)_ during Play 2~~. The Under Ice float has been excluded.~~ Blue stippling indicates _an ice concentration greater than 0%_~~the presence of ice~~ on 15 September 2022, as determined from the MASIE-NH ice product.**

3.3 Play #3: Ice survey

720   On 16 September the _RV Woldstad_ entered the sea ice to avoid heavy seas as Typhoon Merbok hit the Bering Strait (Figure 4~~7~~6 and 4~~8~~7). One HydroBuoy was deployed, and two SWIFTs and JetSSP were deployed in moderate ice cover to examine small-scale gradients within the sea ice. Aircraft flights 3 and 4 (Table 9) over Wave Gliders to the southwest were carried out over two days.
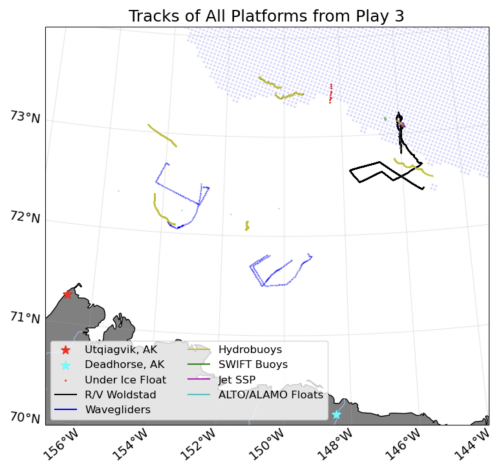
725

Figure 4~~7~~6. A map showing the tracks of all six platforms during Play 3. Blue stippling indicates an ice concentration greater than 0%~~the presence of ice~~ on 17 September 2022, as determined from the MASIE-NH ice product.

a   b
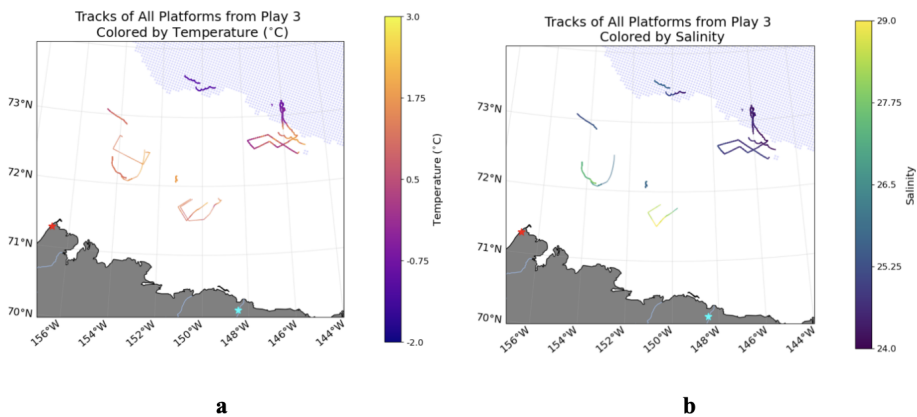
Figure 4~~8~~7. (a) Temperature ~~(a)~~ and (b) salinity ~~(b)~~ recorded closest to the sea surface by each asset (except UIF) during Play 3. ~~The Under Ice float has been excluded.~~ Blue stippling indicates an ice concentration greater than 0%~~the presence of ice~~ on 17 September 2022, as determined from the MASIE-NH ice product.

730

3.4 Play #4: Drifter-following boxes

Play 4 focused on capturing the spatio-temporal variability of a strong surface salinity front in open water. On 19 September, five assets were deployed in a north-south line across the gradient. As these assets drifted north-westward

735 with the gyre circulation on the following three days, the ship steamed in a series of overlapping boxes around them (Figure 498), collecting continuous uCTD measurements and deploying the JetSSP next to the ship to provide measurements from the surface down to ~100 m. Additional SWIFTs were deployed on 21 and 22 September to target strong salinity gradients<s>signals of interest</s>. Strong sub--mesoscale fronts were observed, with significant variability in both space and time (Figure 5049).
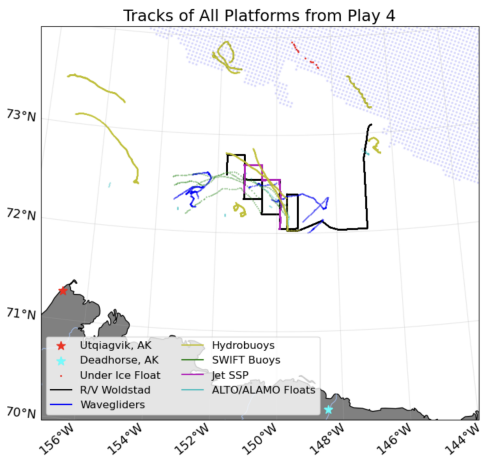
740

Figure 498. A map showing the tracks of all six platforms during Play 4. Blue stippling indicates an ice concentration greater than 0%<s>the presence of ice</s> on 21 September 2022, as determined from the MASIE-NH ice product.

c d
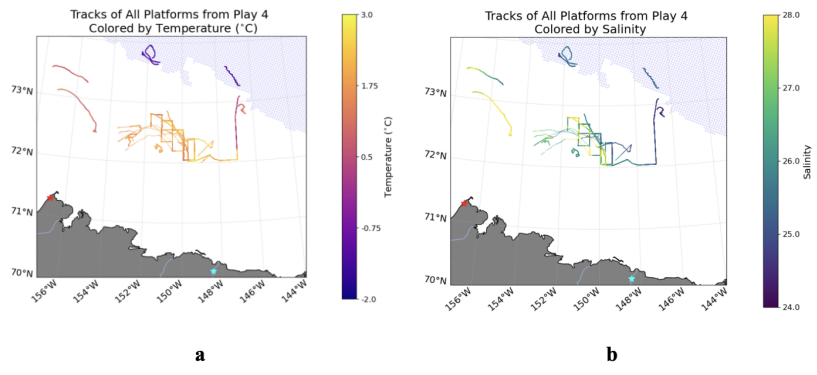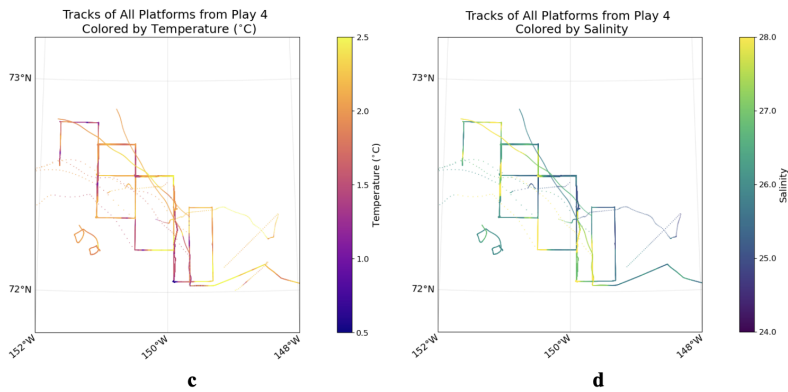
745 **Figure 5049. (a) Temperature (a) and (b) sSalinity (b) recorded closest to the sea surface by each asset (except UIF) during Play 4. The Under Ice float has been excluded. A zoomed in view of the temperature (c) and salinity (d) recorded by the drifter following boxes is also shown. Blue stippling indicates an ice concentration greater than 0% the presence of ice on 21 September 2022, as determined from the MASIE-NH ice product.**

750 **3.5 Play #5: Transects across ice-open water transition**

The final play targeted the open water-sea ice transition immediately prior to freeze-up (Figure 510). Over four days, the ship made 14 consecutive transects along 150°30'W collecting uCTD measurements that captured the evolution of the upper ocean as it moved toward the freezing point. Wave Gliders made north-south transects on either side of the ship, and measurements with drifting assets and JetSSP were also collected. Figure 521 shows a single section of

755 uCTD data: notable features include a near-surface temperature maximum around 10-20 m depth that is maintained by the fresh surface layer; lateral variability above the pycnocline around 20 m depth, with the presence of temperature fronts coinciding with the transition into sea ice; and patchy Pacific summer water signals (warm water at 50-80 m depth) observed south of the ice edge; and vertical variability around 73.15°N.

Tracks of All Platforms from Play 5
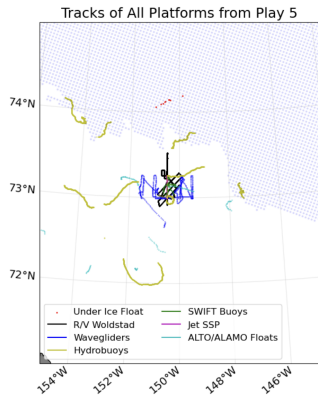
760   **Figure 5̶1̶0̶. A Map showing the tracks of all six platforms during Play 5. Blue stippling indicates an ice concentration greater than 0% ̶t̶h̶e̶ ̶p̶r̶e̶s̶e̶n̶c̶e̶ ̶o̶f̶ ̶i̶c̶e̶ on 27 September 2022, as determined from the MASIE-NH ice product.**
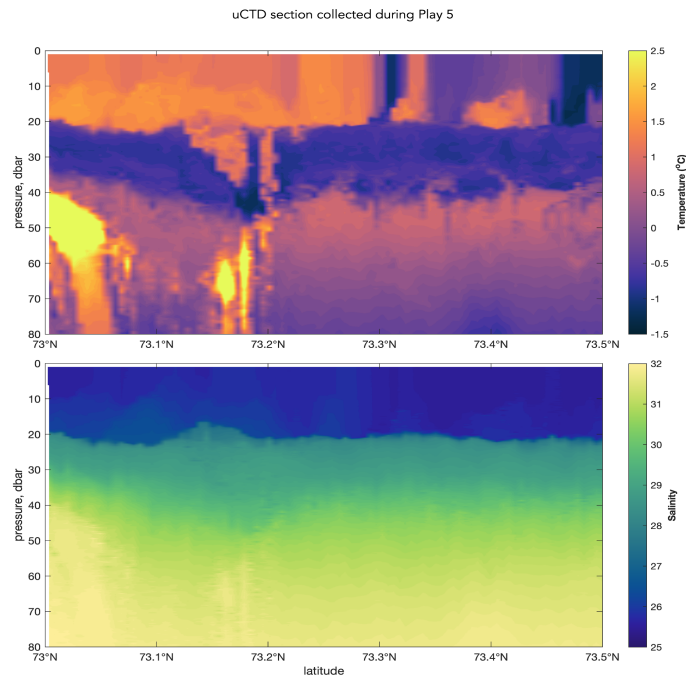
uCTD section collected during Play 5

Figure 5̶2̶1̶. (top) Temperature and (bottom) salinity collected with the uCTD along 150°30'̶W during one section of Play 5 on 25 September. During this transect, sea ice was observed north of around 73.3°N ̶(̶7̶3̶°̶1̶8̶'̶N̶)̶, with open water observed
765   **to the south.**

4. Data Access

Table 11 gives information about where to access the data described in this paper. ~~The SASSIE datasets described in this paper are listed inTable 11~~~~The following gives DOIs describing where to access SASSIE data can be accesse~~All datasets have been quality controlled by the investigators who collected the dataset: details about processing of some of them are described in the papers listed in Table 11. ~~based on procedures appropriate for that dataset. are~~ The datasets are considered to be processed and calibrated (~~,~~ i.e., level 2~~; (L2),~~ except where indicated. Data are accessed using https://doi.org/ [DOI], where [DOI] for each dataset is shown below. The full SASSIE data archive is also accessible via PO.DAAC, https://podaac.jpl.nasa.gov/SASSIE Access to level 0 (L0) data can be obtained by contacting PO.DAAC at podaac@nasa.jpl.gov. Additional information about the Wave Glider, ALTO/ALAMO, and SWIFT datasets can be found at their respective DOIs~~the DOIs below~~ under 'Documentation'. All data files include CF-compliant metadata describing the instruments.

Dataset	DOI	Citation for additional processing and/or quality control procedure details
Shipboard data		
TSG	10.5067/SASSIE-TSG2	N/A
Meteorology and air-sea flux	10.5067/SASSIE-MET2	Edson et al. (1998), Edson et al. (2013)
Salinity Snake	10.5067/SASSIE-SNK2	Ho and Schanze (2020)
ADCP	10.5067/SASSIE-ADCP2	N/A
Underway CTD	10.5067/SASSIE-UCTD2	N/A
Castaway CTD	10.5067/SASSIE-RVCTD2	N/A
S-band radar L3	10.5067/SASSIE-SBAND3	Thompson et al. (2019)
S-band radar L4	10.5067/SASSIE-SBAND4	N/A
$\delta18O$~~$\delta^{18}O$~~	10.5067/SASSIE-D18O2	N/A
Piloted/drifting data		
Wave Gliders	10.5067/SASSIE-GLID2	Thomson et al/. (2018)
JetSSP	10.5067/SASSIE-JETSSP2	Drushka et al. (2019)
SWIFT	10.5067/SASSIE-SWFT2	Thomson et al. (2012)
HydroBuoys	10.5067/SASSIE-HYDROGRAPHY2	Banzon et al. (2020)

ALTO/ALAMO	10.5067/SASSIE-PFLT2	Wong et al. (2020)	
Under-ice float	10.5067/SASSIE-ICFLT2	N/A	
Aircraft data			
PALS L1	10.5067/SASSIE-PALS1	Ogut et al. (2024)	
PALS L2	10.5067/SASSIE-PALS2	Ogut et al. (2024)	

Table 11. DOIs for each of the published SASSIE datasets, plus additional references if available.

5. Abbreviation Glossary

Abbreviation	Stands for…
ADCP	Acoustic Doppler Current Profiler
AIS	Automatic Identification System
ALTO	A profiling float manufactured by Marine Robotic Vehicles
ALAMO	Air Launched Autonomous Micro-Observer
AMSR	Advanced Microwave Scanning Radiometer
APL-UW	Applied Physics Laboratory, University of Washington of UW
CDOM	Colored Dissolved Organic Matter
CT	Conductivity and Temperature
C-FLUOR probe	Turner Designs fluorescence probe
COARE	Coupled Ocean Atmosphere Response Experiment
cCTD	Castaway Conductivity Temperature Depth Sensor
DCFS	Direct Covariance Flux System
DOI	Digital Object Identifier
ETOPO2	National Centers for Environmental Information Topography and Bathymetry Global Relief Model
FDOM	Fluorescent Dissolved Organic Matter
GeoTIFF	Geographical Flag Image File Format
GPCTD	Glider Payload Conductivity Temperature, Depth Sensor
GPS	Global Positioning System

IMU	Inertial motion unit
JetSSP	Jet-driven Surface Salinity Profiler
MASIE	Multisensor Analyzed Sea Ice Extent (US National Ice Center, 2010)
MIZ	Marginal Ice Zone
MET	Meteorology
NASA	National Aeronautics and Space Administration
PALS	Passive Active L-band System
PO.DAAC	Physical Oceanography Distributed Active Archive Center
RBR	Name of a brand making submersible sensors for both physical and biological ocean variables.
RHRV	Relative humidityResearch Vessel
RVRH	Research VesselRelative humidity
SASSIE	Salinity and Stratification at the Sea Ice Edge
SBE	Sea-Bird Electronics
SeaCAT	Sea Bird CTD model
SMAP	Soil Moisture Active Passive
SSP	Surface salinity profiler
SSS	Sea Surface Salinity
SST	Sea Surface Temperature
SV3	Surface Vehicle Model 3
SWIFT	Surface Wave Instrument Floats with Tracking
TKE	Total Kinetic Energy
TSG	Thermosalinograph
uCTD	Underway Conductivity Temperature Depth Sensor
UIF	Under Ice Float
USV	Unmanned Surface Vessel

~~UW~~	~~University of Washington~~
~~VMDAS~~	~~Vessel Mounted Data Acquisition System~~
WHOI	Woods Hole Oceanographic Institut~~e~~ion

Table 12. Glossary of abbreviations and acronyms used throughout the paper.

Author contribution

KD and PG led the SASSIE ~~overall~~ project, with KD leading through the cruise and PG leading the post-cruise work. KD wrote sections 1, 3, and 4 of the manuscript. EW co-wrote~~prepared~~ the manuscript and prepared the~~,~~ figures~~,~~ and code, with contributions from all co-authors. FMB and EW led the data publication. KD led collection and processing of the TSG, JetSSP, S-band Radar, and δ18O~~δ18O~~ data. PG and CS led collection and processing of the uCTD data. PG, EJR, and JT led collection and processing of the ADCP data. PG and JP led collection and processing of the cCTD data. SD and MS led collection and processing of the HydroBuoy data. MS organized deployment of the ALAMO and ALTO float data. SF and SM led collection and processing of the PALS data. VM and SZ led collection and processing of the meteorology and air-sea flux data. JT and EJR led collection and processing of the Wave Glider and SWIFT data. JJS led collection and processing of the salinity snake data. AS led collection and processing of the under-ice float data.

Code availability

Code used to read the SASSIE data and generate the figures from this manuscript is available as~~in~~ Jupyter notebooks at https://github.com/lizwestbro/SASSIE_Data.

Acknowledgements

The SASSIE Program was supported by NASA Award 80NSSC21K0832. We are ~~extremely~~ grateful to the Captains and Crew of the RV *Woldstad* and to Support Vessels of Alaska, as well as the pilots of Kenn Borek Air, for enabling us to collect these data. We thank Justin Burnett, Alex de Klerk, Léa Olivier and Laëtitia Parc for helping collect data on the SASSIE expedition, and Ian Fenty and Mehmet Ogut for helping collect SASSIE aircraft data. ALAMO and ALTO floats were provided, and the data organized by S. Jayne and A. Ekholm (WHOI) and J. Kerling (NAVOCEANO).

References

Banzon, V., Smith T.M., Steele M., Huang B., and Zhang H.: Improved Estimation of Proxy Sea Surface Temperature in the Arctic, J. Atmos. Ocean. Tech., 37, 341–349, https://doi.org/10.1175/JTECH-D-19-0177.1, 2020.

Castro, S., Wick G., and Steele M.: Validation of satellite sea surface temperature analyses in the Beaufort Sea using UpTempO buoys, Rem. Sens. Environ., 187, 458-475, https://doi.org/10.1016/j.rse.2016.10.035, 2016.

Cox, G.F. and Weeks, W.F.: Salinity variations in sea ice. Journal of Glaciology, 13(67), pp.109-120, 1974.

Crews, L., Lee C.M., Rainville L., and Thomson, J.: Direct observations of the role of lateral advection of sea ice meltwater in the onset of autumn freeze up. J. Geophys. Res-Oceans, 127, https://doi.org/10.1029/2021JC017775, 820   2022.

D'Asaro, E. A.: Performance of autonomous Lagrangian floats. J. Atmos. Ocean. Tech., 20, 896–911, https://doi.org/10.1175/1520-0426(2003)020<0896:POALF>2.0.CO;2, 2003.

825   Dewey, S. R., Morison J.H., and Zhang J.: An Edge-Referenced Surface Fresh Layer in the Beaufort Sea Seasonal Ice Zone. J. Phys. Oceanogr., 47, 1125–1144, https://doi.org/10.1175/JPO-D-16-0158.1, 2017.

Drushka K., Asher W.E., Jessup A.T., Thompson E.J., Iyer S., and Clark D. Capturing fresh layers with the surface salinity profiler. Oceanography. 32(2):76-85, https://doi.org/10.5670/oceanog.2019.215, 2019.
830

Drushka, K.: SASSIE Arctic Field Campaign Shipboard Thermosalinograph Data Fall 2022. Ver. 1. PO.DAAC, CA, USA. https://doi.org/10.5067/SASSIE-TSG2, 2023a.

Drushka, K.: SASSIE Arctic Field Campaign Shipboard S-Band Radar Level 3 Data Fall 2022. Ver. 1. PO.DAAC, 835   CA,   USA.   https://doi.org/10.5067https://doi.org/10.5067/SASSIE-SBAND3/SASSIE_L3_SHIPBOARD_SBAND_V1, 2023b.

Drushka, K.: SASSIE Arctic Field Campaign Shipboard S-Band Radar Level 4 Data Fall 2022. Ver. 1. PO.DAAC, CA, USA. https://doi.org/10.5067/SASSIE-SBAND4, 2023c.
840
Drushka, K.: SASSIE Arctic Field Campaign Shipboard Delta-18O Data Fall 2022. Ver. 1. PO.DAAC, CA, USA. https://doi.org/10.5067/SASSIE-D18O2, 2023de.

Drushka, K.: SASSIE Arctic Field Campaign Jet Surface Salinity Profiler Data Fall 2022. Ver. 1. PO.DAAC, CA, 845   USA. https://doi.org/10.5067/SASSIE-JETSSP2, 2023ed.

Edson, J.B., et al.: A study of the inertial-dissipation method for computing air-sea fluxes. J. Geophys. Res-Oceans, 96 10689-10711. https://doi.org/10.1029/91JC00886, 1991.

850   Edson, J.B., et al.: Direct covariance flux estimates from mobile platforms at sea. J. Atmos. Ocean. Tech. 15.2, 547-562, https://doi.org/10.1175/1520-0426(1998)015<0547:DCFEFM>2.0.CO;2, 1998.

Edson, J.B., et al.: On the exchange of momentum over the open ocean. J. Phys. Oceanogr. 43.8, 1589-1610, https://doi.org/10.1175/JPO-D-12-0173.1, 2013

855

Fairall, C.W., and Markson R.: Mesoscale variations in surface stress, heat fluxes, and drag coefficient in the marginal ice zone during the 1983 Marginal Ice Zone Experiment. J. Geophy Res-Oceans, 92.C7, 6921-6932, https://doi.org/10.1029/JC092iC07p06921, 1987.

860 Fairall, C.W., et al.: Inertial-dissipation air-sea flux measurements: a prototype system using real time spectral computations. J. Atmos. Ocean. Tech. 7.3, 425-453, https://doi.org/10.1175/15200426(1990)007<0425:IDASFM>2.0.CO;2 , 1990.

Gaube, P.: SASSIE Arctic Field Campaign Shipboard ADCP Data Fall 2022. Ver. 1. PO.DAAC, CA, USA.
865 https://doi.org/10.5067/SASSIE-ADCP2, 2023.

Haykin, S., Currie, B.W., Lewis, E.O., & Nickerson, K.A.: Surface-based radar imaging of sea ice. Proceedings of the IEEE, 73(2), 233-251, https://doi.org/10.1109/PROC.1985.13136, 1985.

870 -Ho, D. T., & Schanze, J. J.: Precipitation-Induced Reduction in Surface Ocean pCO2: Observations From the Eastern Tropical Pacific Ocean. Geophys. Res. Lett, 47, https://doi.org/10.1029/2020GL088252, 2020.

Jackson, J.M., Carmack, E.C., McLaughlin, F.A., Allen, S.E. and Ingram, R.G.: Identification, characterization, and change of the near-surface temperature maximum in the Canada Basin, 1993–2008. J Geophys Res-Oceans, 115,
875 https://doi.org/10.1029/2009JC005265, 2010.

Jayne, Steve: SASSIE Arctic Field Campaign ALTO/ALAMO Profiling Float Data Fall 2022. Ver. 1. PO.DAAC, CA, USA. https://doi.org/10.5067/SASSIE-PFLT2, 2023.

880 Lannuzel, D., Tedesco, L., van Leeuwe, M. et al.: The future of Arctic sea-ice biogeochemistry and ice-associated ecosystems. Nat. Clim. Chang. 10, 983–992, https://doi.org/10.1038/s41558-020-00940-4, 2020

Lansard, B., Mucci, A., Miller, L.A., Macdonald, R.W. and Gratton, Y.. Seasonal variability of water mass distribution in the southeastern Beaufort Sea determined by total alkalinity and δ18O. J. of Geophys Res-Oceans, 117(C3),
885 https://doi.org/10.1029/2011JC007299, 2012.

Lund, B., Graber, H. C., Persson, P. O. G., Smith, M., Doble, M., Thomson, J., et al.: Arctic sea ice drift measured by shipboard marine radar. J. Geophys. Res-Oceans, 123, 4298–4321. https://doi.org/10.1029/ 2018JC013769, 2018.

890   Menezes, M and Zippel, S: SASSIE Arctic Field Campaign Shipboard Meteorology Data Fall 2022. Ver. 1. PO.DAAC, CA, USA. https://doi.org/10.5067/SASSIE-MET2, 2023.

895   M. Ogut, S. Misra, X. Bosch-Lluis, I. Ramos, R. Williamson, C.S. Chae, A. Colliander and S. Yueh: Development and Testing of a Combined Active/Passive Microwave Remote Sensing Instrument. (Under review at IEEE JSTARS), 2024.

Perez Valentin, J.: SASSIE Arctic Field Campaign Castaway Data Fall 2022. Ver. 1. PO.DAAC, CA, USA. https://doi.org/10.5067/SASSIE-RVCTD2, 2023.

900   Persson, P. Ola G., et al.: Shipboard observations of the meteorology and near-surface environment during autumn freeze up in the Beaufort/Chukchi Seas. J. Geophys. Res-Oceans, 123.7, 4930-4969, https://doi.org/10.1029/2018JC013786, 2018

Schanze, Julian: SASSIE Arctic Field Campaign Shipboard Salinity Snake Data Fall 2022. Ver. 1. PO.DAAC, CA,
905   USA. https://doi.org/10.5067/SASSIE-SNK2, 2023.

Schlundt, Michael, et al: Accuracy of wind observations from open-ocean buoys: Correction for flow distortion. J Atmos Ocean Technol. 37.4, 687-703, https://doi.org/10.1175/JTECH-D-19-0132.1, 2020.

910   Schmidgall, C.: SASSIE Arctic Field Campaign Shipboard Underway CTD Data Fall 2022. Ver. 1. PO.DAAC, CA, USA. https://doi.org/10.5067/SASSIE-UCTD2, 2023.

Shcherbina, Andrey: SASSIE Arctic Field Campaign Under-Ice Float Data Fall 2022. Ver. 1. PO.DAAC, CA, USA. https://doi.org/10.5067/SASSIE-ICFLT2, 2023.
915

Smith, A., and Jahn, A.: Definition differences and internal variability affect the simulated Arctic sea ice melt season. The Cryosphere 13, 1–20, https://doi.org/10.5194/tc-13-1-2019, 2019.

Smith M., Stammerjohn S., Persson O., Rainville L., Liu G., Perrie W., Robertson R., Jackson J., and Thomson J.:
920   Episodic Reversal of Autumn Ice Advance Caused by Release of Ocean Heat in the Beaufort Sea. J. Geophys Res-Oceans, 123, 3164–85. https://doi.org/10.1002/2018JC013764, 2018.

Steele, Michael: SASSIE Arctic Field Campaign Drifter Hydrography Data Fall 2022. Ver. 1. PO.DAAC, CA, USA. https://doi.org/10.5067/SASSIE-UPTEMPO2, 2023.
925

Stroeve, J.C., Crawford A.D., and S. Stammerjohn S.: Using timing of ice retreat to predict timing of fall freeze-up in the Arctic. Geophys. Res. Lett., 43(12), 6,332–6,340, https://doi.org/10.1002/2016GL069314, 2016.

930 Stroeve, J.C., Markus T., Boisvert L., Miller J., and Barrett A.: Changes in Arctic melt season and implications for sea ice loss. Geophys. Res. Lett. 41(4), 1,216–1,225, https://doi.org/10.1002/2013GL058951, 2014

Stroeve, J., and Notz D.: Changing state of Arctic sea ice across all seasons. Environ. Res. Lett., 13(10), 103001, https://doi.org/10.1088/1748-9326/aade56, 2018.

935 Thompson EJ, Asher WE, Jessup AT, Drushka K. High-resolution rain maps from an X-band marine radar and their use in understanding ocean freshening. Oceanography. 32(2):58-65, https://doi.org/10.5670/oceanog.2019.213, 2019.

Thomson, J.: Observations of wave breaking dissipation from a SWIFT drifter. J. Atmos. Ocean. Tech., 29, 1866-1882, https://doi.org/10.1175/JTECH-D-12-00018.1, 2012.

940 Thomson, J., J. B. Girton, R. Jha, and A. Trapani. Measurements of Directional Wave Spectra and Wind Stress from a Wave Glider Autonomous Surface Vehicle. J. Atmos. Oceanic Technol., 35, 347–363, https://doi.org/10.1175/JTECH-D-17-0091.1, 2018.

945 Thomson J.: SASSIE Arctic Field Campaign Wave Glider Data Fall 2022. Ver. 1. PO.DAAC, CA, USA. https://doi.org/10.5067/SASSIE-GLID2, 2023a

Thomson, J.: SASSIE Arctic Field Campaign SWIFT Data Fall 2022. Ver. 1. PO.DAAC, CA, USA. https://doi.org/10.5067/SASSIE-SWIFT2, 2023b.

950

Thomson, J., and Girton J.: Sustained measurements of Southern Ocean air-sea coupling from a Wave Glider autonomous surface vehicle. Oceanography, 30, 104–109, https://doi.org/10.5670/oceanog.2017.228, 2017.

Thomson, J., Girton J., Jha R., Trapani A.: Measurements of Directional Wave Spectra and Wind Stress from a Wave 955 Glider Autonomous Surface Vehicle. J. Atmos. Ocean. Tech., 35, 347-363, https://doi.org/10.1175/JTECH-D-17-0091.1, 2018.

U.S. National Ice Center, F. Fetterer, M. Savoie, S. Helfrich, and P. Clemente-Colón. (2010). Multisensor Analyzed Sea Ice Extent - Northern Hemisphere (MASIE-NH), Version 1 4km. Boulder, Colorado USA. National Snow and 960 Ice Data Center. https://doi.org/10.7265/N5GT5K3K. Date Accessed 09-21-2023.

Viva Banzon, Thomas M Smith, Michael Steele, Boyin Huang, & Huai-Min Zhang. Improved Estimation of Proxy Sea Surface Temperature in the Arctic. Journal of Atmospheric and Oceanic Technology. Vol. 37. pp. 341-349. doi:10.1175/JTECH-D-19-0177.1, 2020.

965

Wilson, W.J., Yueh, S.H., Dinardo, S.J., Chazanoff, S.L., Kitiyakara, A., Li, F.K. and Rahmat-Samii, Y.: Passive active L-and S-band (PALS) microwave sensor for ocean salinity and soil moisture measurements. IEEE Transactions on Geoscience and Remote Sensing, 39(5), 1039-1048, https://doi.org/10.1109/36.921422, 2001.

970   Wilson, W.J., Yueh, S.H., Li, F.K., Dinardo, S., Chao, Y., Koblinsky, C., Lagerloef, G. and Howden, S.: Ocean surface salinity remote sensing with the JPL Passive/Active L-/S-band (PALS) microwave instrument. In IGARSS 2001. Scanning the Present and Resolving the Future. Proceedings. IEEE 2001 International Geoscience and Remote Sensing Symposium (Cat. No. 01CH37217), 2, 937-939, https://doi.org/10.1109/IGARSS.2001.976686, 2001.

975   Wong, A.P., Wijffels, S.E., Riser, S.C., Pouliquen, S., Hosoda, S., Roemmich, D., Gilson, J., Johnson, G.C., Martini, K., Murphy, D.J. and Scanderbeg, M.. Argo data 1999–2019: Two million temperature-salinity profiles and subsurface velocity observations from a global array of profiling floats. Frontiers in Marine Science, 7, p.700, https://doi.org/10.3389/fmars.2020.00700, 2020.

980   Yueh, S.H. and Chaubell, J.: Sea surface salinity and wind retrieval using combined passive and active L-band microwave observations. IEEE transactions on geoscience and remote sensing, 50(4), .1022-1032, https://doi.org/10.1109/TGRS.2011.2165075, 2011.

985